OSLO METROPOLITAN UNIVERSITY
STORBYUNIVERSITET

Master's Degree in
Structural Engineering and Building Technology
Department of Civil Engineering and Energy Technology

ACCESSIBILITY
OPEN

MASTER THESIS

THESIS TITLE	**DATE** **15.06.2020**
Impact of Dynamic Wind on Fan Pressurization Method for Determination of Building Airtightness	**NUMBER OF PAGES: 52** **NO.OF ATTACHMENT: 43**
AUTHOR **Feyu Kebede Kolstad**	**SUPERVISOR** **Dimitrios Kraniotis** Associate Professor Dep. of Civil Engineering and Energy Technology Oslo Metropolitan University - OsloMet

IN COLLABORATION WITH	**CONTACT PERSON**
OSLO METROPOLITAN UNIVERSITY	**Feyu Kebede Kolstad**

SUMMARY
Building infiltration is identified as a major contributor for heat loss, and as one of the factors that have a great impact on the airtightness of a built environment. An accurate evaluation of the airtightness level, however, demands an optimised estimation of uncertainties that may arise due to the dynamic wind during measurement. The purpose of this thesis is therefore to investigate and characterize the airtightness of a building envelope with respect to varying wind conditions. Coefficient of determination, which qualifies the relationship between building pressure and the building leakage, is selected to quantify any observable dynamic wind impact and consequences thereon. The analysis of the results indicate that the impact assessment of dynamic wind condition shall consider the following factors; 1)angular exposure of the blower door to the direction of the prevailing wind speed, 2) spectral energy distribution at low frequencies, and 3) the wind speed carrying the maximum energy. Further more, for an accurate description of the dynamic wind condition, the best fitting distribution function must be systematically selected. A good criteria for selection of such distribution function is suggested to combine the wind speed and wind direction parameters. Finally, among the values of coefficients of determination that were found to be satisfactory according to the current ISO9972:2015 standard, mean wind speed up to $V_{xy} \approx 4.8 m/s$ with corresponding wind speeds that carry maximum energy of $V_{xy_{MaxE}} \approx 5.8 m/s$ were reported. This implicates the approach utilized by ISO9972 as a rather conservative design.

3 KEYWORDS
Dynamic wind
Coefficient of determination
Fan pressurization method

Impact of Dynamic Wind on Fan Pressurization Method for Determination of Building Airtightness

Feyu Kebede Kolstad

Abstract

Since the early 2000's, the member states of the European Union (EU) and European Economic Area (EEA), have been engaged in an effort to account for air infiltration through the building envelope. Building infiltration is identified as a major contributor for heat loss, and as one of the factors that have a great impact on the the airtightness of a built environment. A standard the airtightness evaluation procedure is known as the fan pressurization method is established. An accurate evaluation of the airtightness level, however, demands an optimised estimation of the uncertainties related to the measurement method.

Despite halve a century worth of application, a knowledge gap remains an untended concerning the quantification of uncertainties due to the impact of dynamic wind on fan pressurization method. The purpose of this thesis is therefore to investigate and characterize the airtightness of a building envelope with respect to varying wind conditions. Coefficient of determination, which qualifies the relationship between building pressure and the building leakage, is selected to quantify any observable dynamic wind impact and consequences thereon.

The experimental study was conducted at the field station for bio-climatic studies at the Norwegian University of Life Science (NMBU) in Ås, Norway. A Minneapolis Blower Door system is used to measure the building pressures across the envelope. The Blower Door Test procedure known as a Multi-Point Test was performed in testing the building over a range of target pressures. The wind data in the dynamic condition was captured by an ultrasonic anemometer device. It was located at a distance of 20m without any obstruction within a radius of ca 18m, at a height of 2.2m above the ground. The wind data was further processed numerically by MATLAB@ programming software. Normal and Weibull probability density models were simulated to quantify and investigate the natural distribution pattern. A spectral density estimation is also performed to quantify the energy distribution of the dynamic wind signal in a frequency spectrum.

The analysis of the results indicate that the impact assessment of dynamic wind condition shall consider the following factors; 1)angular exposure of the blower door to the direction of the prevailing wind speed, 2) spectral energy distribution at low frequencies, and 3) the wind speed carrying the maximum energy. Further more, for an accurate description of the dynamic wind condition, the best fitting distribution function must be systematically selected. A good criteria for selection of such distribution function is suggested to combine the wind speed and wind direction parameters. Finally, among the values of coefficients of determination that were found to be satisfactory according to the current ISO9972:2015 standard, mean wind speed up to $V_{xy} \approx 4.8m/s$ with corresponding wind speeds that carry maximum energy of $V_{xy_{MaxE}} \approx 5.8m/s$ were reported. this outcome implicates the approach utilized by ISO9972 as a rather conservative design.

To Marte
To Kenna
To Naol

And
To our soon born

Acknowledgment

I would like to express my gratitude to my supervisor Dimitrios Kraniotis for the continual comments, encouragement and engaging discussions through out the making of this master thesis. Furthermore I would like to thank Tormod Aurlien and Signe Kroken from the Norwegian University of Life Sciences(NMBU), for their cooperation and facilitating access to the experiment site. Also, I would like to thank my classmates, Class of Fall 2018, for two memorable years which I cherish. What a journey!

I would like to thank my loved ones, and acknowledge the support and great love of my family, my wife, Marte; my two sons, Kenna and Naol; my parents Kebede and Netsanet; my siblings, Gedion, Natoli and Sinhawe; My freinds, Derara, Henock, Jigsa and Torben; My family in law who have been part of this journey from the start. Thank you for your support throughout entire process. I will be grateful forever for your love.

Feyu Kebede Kolstad

Oslo, 15.june 2020

Contents

List of Figures

List of Tables

Chapter 1

Introduction

1.1 Background

In Europe, around 40% of the total energy use comes from buildings, of which more than 30% are catagorized as historical buildings (Favi et al., 2018). It is estimated that almost 50% of the total final energy consumption (TFC) of the union is used for heating and cooling. The demand for heating and cooling of buildings is approximated to represent 80% of the total final energy consumption (TFC) (European Parliament, 2018). In an effort to develop a sustainable, competitive, secure and decarbonised energy system, the European Union has taken the steps to legislate and implement energy efficiency acts, including the Energy Performance of Buildings Directive (EPBD). The directive recommends and promotes nearly zero-energy buildings (nZEB) and related best practices to ensure that, by year 2020, all new buildings are nearly zero-energy buildings. New buildings are being designed to fulfill these requirements with newly adopted standards reflecting various ZEB ambition levels (Brit Roald, 2017). The directive also encourages research into and testing of new solutions for improving the energy performance of historical buildings and sites, while also safeguarding and preserving cultural heritage. The overall target is to reduce the energy consumption and thereby the gas emissions from the building stock.

Recent data from the International Energy Agency (IEA) reveals that the total final energy consumption (TFC) of Norway's residential buildings represent 19% of the total consumption amongst the sectors (IEA, 2017) (See figure1.1). As Norway aims to be carbon neutral by 2030 and a low-emission[1] society by 2050, decreasing the energy consumption from all sectors is a priority. Specially the contribution from the building stock can be significant.

In this regard, one of the factors that have a great impact on the thermal performance of a built environment is the extent of air infiltration through the building envelope (Poza-Casado et al., 2019; Jesús et al., 2019; Jokisalo et al., 2009). Building infiltration is identified as a major contributor for heat loss, even more so than those caused by transmission through the building envelope (Zou, 2010). It is also disturbs the designed function of mechanical ventilation, resulting either to additional energy use or poor indoor air quality. Consequently, the mechanisms governing building's air tightness and the impact of air infiltrations on energy has increasingly become an areas of scientific research (Leprince et al., 2017). Achieving an optimal thermal comfort, improving indoor air quality and increasing performance of ventilation systems are concurrently identified by the literature as rationals for growing focus on buildings airtightness (Poza-Casado et al., 2019; Jesús et al., 2019; Zou, 2010; Leprince et al., 2017; Bracke et al., 2016). The literature also identifies challenges related to moisture such as occurrence of condensation, and growth of mold and rot. Hence, it necessitates a special consideration to airtightness in designing

[1] Emissions levels of 80-95% below the 1990 levels

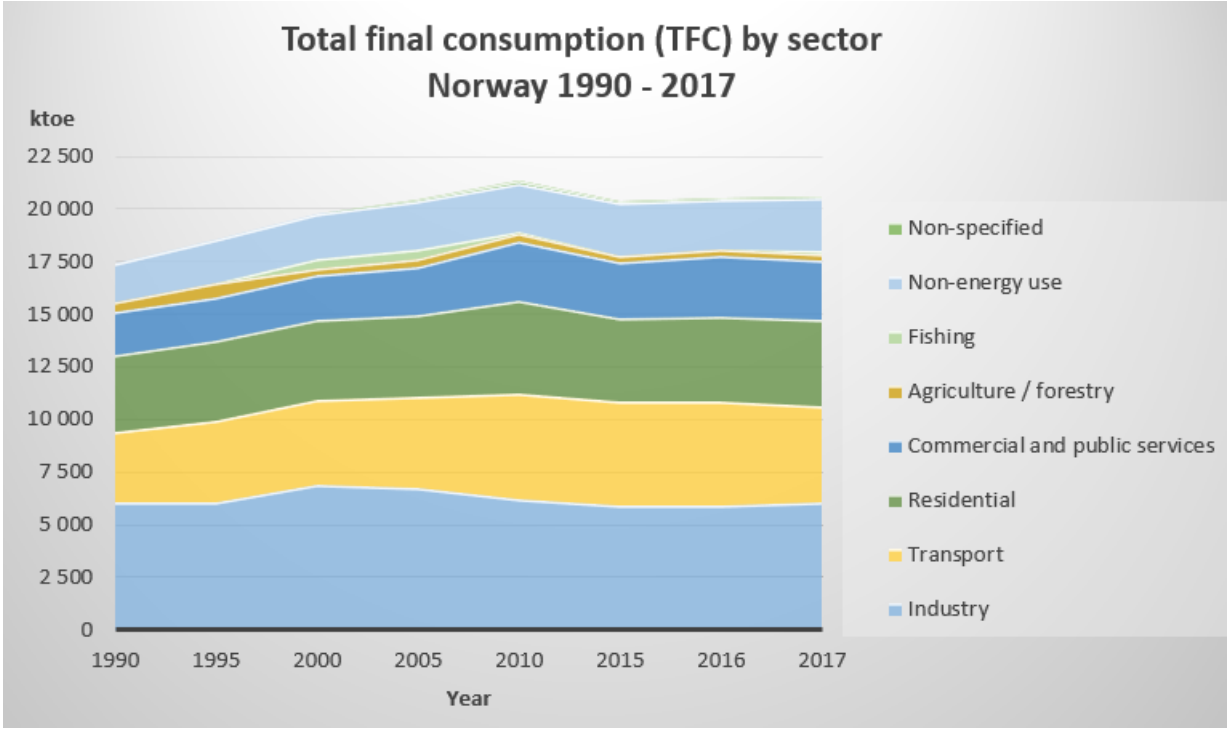

Figure 1.1: The final energy consumption in Norway (source: IEA, 2020)

and construction of buildings.

Since the early 2000's, the member states of the European Union (EU) and European Economic Area (EEA), have been engaged in an effort to account for airtightness (Bracke et al., 2016). This was strengthened by the emergence of EU directives (European Parliament, 2018) and a guiding document issued by EU for energy target and policies, also known as 'Energy Roadmap 2050' (European Commission, 2011).

A standard method is therefore established in order to determine the airtightness of a building. The NS-EN ISO 9972:2015 standard employs the blower door test to characterize airtightness (CEN, 2015). An accurate evaluation of the airtightness level, however, demands an optimised estimation of the uncertainties related to the measurement method. Despite halve a century worth of application, a knowledge gap remains an untended concerning the quantification of uncertainties related to the test method (Prignon et al., 2019). As this is crucial in conducting a more correct calculation of the energy footprint of infiltration, researches have been conducted on probable sources of uncertainties. Sources identified by the literature may include, the applied regression methods on zero-flow pressure (Prignon et al., 2018, 2019; Delmotte, 2017), and factors such as steady wind (Leprince & Carrié, 2018) are identified in the literature.

In envelope airtightness measurements, the impact of wind and more generally of climatic conditions are taken into account through the calculation of zero-flow pressure. However, climatic conditions, and in turn the zero-flow pressure, do not remain constant during the blower door test. As such the airtightness measurement approach becomes a source of uncertainty that can not be disregarded as the assumption of zero-flow pressure itself is not always valid.

1.2 Purpose and research questions

1.2.1 Purpose

It can be inferred from the introduction section that the conditions under which airtightness measurements are undertaken may influence the measurement accuracy. Using error propagation calculation, the standard has made an effort to address the uncertainties of all derived quantities used for the final result. However,the uncertainties associated with the circumstances of the actual measurements are not taken into consideration. Variation in wind condition, wind speed and direction, during the testing period could affect the measurement of building airtightness (Zheng et al., 2019). Only a favourable conditions were mentioned without any tangible quantification procedure or suggestion for an acceptable reference interval.

The purpose of this thesis is therefore to investigate and characterize the airtightness of a building envelope with respect to varying wind conditions. Coefficient of determination, which qualifies the relationship between building pressure and the building leakage, is selected to quantify any observable dynamic wind impact and consequences thereon. A qualitative outcome is aimed at based on a quantitative study as a ground work further investigation.

1.2.2 Research question

The research question of this thesis are

- **Towards establishing a valid coefficient of determination, what factors must be evaluated in assessing the influence of dynamic wind on the fan pressurization method?**
- **What approaches can be employed for describing the dynamic wind that may arise during the fan pressurization measurement?**

1.2.3 Research Limitation

- The effect of temperature difference, stack effect, is not considered in the thesis.
- Uncertainty that may arise from workmanship are not taken into account.
- The statistical distribution of the intensity of turbulence of the wind is not calculated.
- The statistical distribution and impact of the vertical direction have not been included.

Chapter 2

Theoretical Background

2.1 Air Infiltration: Introduction

Air infiltration is a non-intended and uncontrolled flow or ventilation of outside air to the internal space of a building through leakages (cracks and/or gaps) in the building fabric (Chan et al., 2013). It arises due to the pressure difference across the envelope of a building, driven either by the influence of outside gusting winds or owning to the difference between inside and outside temperatures (Younes et al., 2012). It is also claimed that the presence of ventilation system further contributes to the driving pressure gradient. The contribution of gusting wind to air infiltration predominates in low-rise buildings, under three-story rise buildings, according to the work of Brownell (as cited by Younes et al., 2012). It is further suggested that in high-rise buildings, the driving force of infiltration is primarily the stack effect. Younes et al. explains stack effect as a phenomenon resulting from the difference in air temperature across the building envelope and height, leading to air buoyancy differences and consequently establishing a pressure difference between the inside and outside of the building. Another major influence on a building and its internal environment comes from the ventilation system, which is known to enhance the pressure difference across the building envelope along with air infiltration. Unless duly managed, infiltrating air carries moisture that impacts the long-term performance of the building material (serviceability), the building's structural integrity (durability), behavior in fire (smoke spread), indoor air quality (distribution of pollutants and microbialreservoirs) and thermal energy (Lstiburek et al., 2002). The impact of air infiltration on the buildings energy consumption is profound as it is estimated to make up one third of the energy losses in a building (Vega Pasos et al., 2019). Thus implying building's air infiltration not only as a crucial element to consider in the process of building design, but also as a relevant research topic (Prignon et al., 2019).

According to Younes et al., the energy impact of air infiltration has been classically evaluated as a product of the infiltrating air mass flow rate, the air-specific heat capacity, and the inside–outside temperature difference. The classical expression for heat loss due to infiltration is given by Eq. 2.1:

$$Q_{\mathrm{inf}} \; = \; \dot{m} C_{\mathrm{p}} (T_{\mathrm{i}} \; - \; T_{\mathrm{o}}) \tag{2.1}$$

where $\mathrm{Q_{inf}}$ represents air infiltration energy load (W), $\dot{m}$ represents air infiltration mass flow rate (kg/s), $\mathrm{T_i}$ represents inside (indoor) room temperature (°C), $\mathrm{T_o}$ represents outside (ambient) temperature (°C), and $\mathrm{C_p}$ represents specific heat of air (J/kg °C).

2.2 Air Infiltration: Driving Mechanism

Air infiltration is highly influenced by the indoor-outdoor pressure difference which is the sum of three components: pressure difference due to stack effect, pressure difference due to the wind, and the pressurization of the ventilation system (Muehleisen & Patrizi, 2013). The pressure difference due to stack effect and wind are identified as a primary components of the driving forces of infiltration (Younes et al., 2012). For the purpose of this thesis, the following section will focus on elaborating the driving mechanisms involving pressure difference due to stack effect and wind. Figure 2.1 illustrates how the pressure differences resulting from the driving mechanisms are summed together. The total pressure can be expressed by Equation 2.2 where by the air flow is directed into the building due to a higher external pressure.

$$\Delta P_{\text{tot}} = \Delta P_{\text{s}} + \Delta P_{\text{w}} + \Delta P_{\text{v}} \tag{2.2}$$

where

- ΔP_{tot} is the total pressure difference [Pa]
- ΔP_{s} is the pressure difference from stack effect [Pa]
- ΔP_{w} is the pressure difference from wind [Pa]
- ΔP_{v} is the pressure difference from ventilation [Pa]

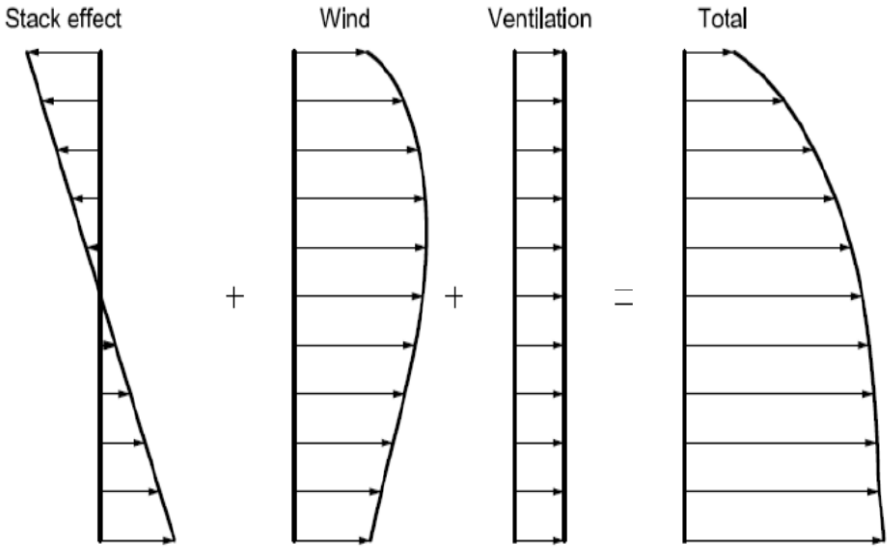

Figure 2.1: Summation of pressure profiles from the three main sources of building pressurization; wind, stack effect and ventilation.

2.2.1 Driving Mechanism: Stack Effect

The stack effect arises as a result of differences in temperature and hence air density between the interior and exterior of a building. It is a movement of air into and out of buildings driven by buoyancy,i.e. due to a difference in indoor-to-outdoor air density resulting from temperature and moisture differences (Khoukhi & Al-Maqbali, 2011). The ideal gal law (Equation 2.3) formulates the mathematical relationship of the temperature and density. Thereby asserting temperature difference across the building envelope as an agent for a respective air density variation:

$$\rho = \frac{P}{RT} \tag{2.3}$$

where ρ represents air density (kg/m3), P represents air pressure (Pa), R represents the specific gas constant, and T represents temperature (°C).

The difference in air density across the building envelope results in a pressure gradient over the height of the structure which is referred to as the 'stack effect' (see figure 2.2). Equation 2.4 defines the 'stack pressure' and its variation with the height of air column along the building envelope at a specific air density ρ (Younes et al., 2012).

$$P = \rho g h \tag{2.4}$$

where g represents gravitational acceleration constant (m/s^2) and h represents height of the air column.

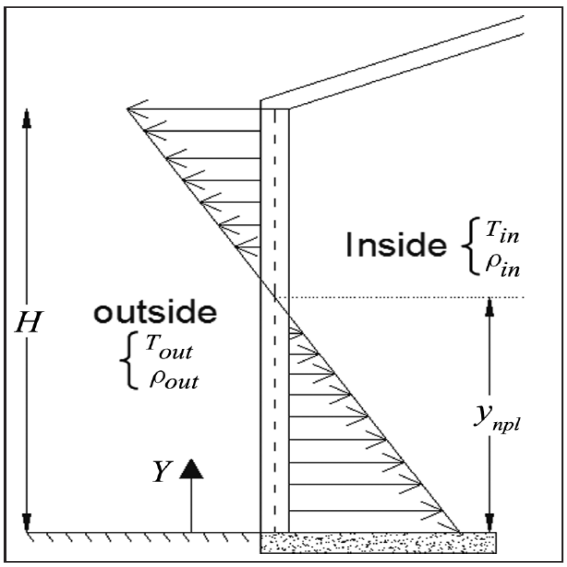

Figure 2.2: Stack effect and neutral pressure line on a building wall (source: Younes et al., 2012)

.

Previous studies (Jo et al., 2007; Khoukhi & Al-Maqbali, 2011; Tamblyn, 1991) have discussed the challenges reported by buildings, especially high rise buildings, as a result of the stack effect. Sticking elevator doors, difficulty in opening doors, and noise resulting from air flowing through cracks can be mentioned as instances of such cases. While improving the overall airtightness of the whole building is considered the most efficient solution, factors such as type and height of buildings and occupant behaviour remain as major determinants of the 'stack effect'. Mechanical ventilation system were proposed as an alternative solution for stack effect-related problems (Tamblyn, 1991). Unfortunately, a study conducted by Lovatt and Wilson, as mentioned in the work of (Yu et al., 2017), revealed that mechanical ventilation system generated the problems one tries to avoind in other parts of the building,

2.2.2 Driving Mechanism: Steady Wind

The impact of a wind pressure on a building structure is related to its intensity, distribution, and nature of the building envelope (Younes et al., 2012). These factors may in turn

vary with the placement of the building. Figure 2.3 depicts a flow of air around a building that creates a wind pressure and the mechanisms involved in inducing pressure difference.

To estimate the wind induced pressure difference, a wind pressure coefficient characterizing the wind intensity, C_p, is required (Muehleisen & Patrizi, 2013). There are three methods to estimate C_p: full-scale test, a model test in a laboratory wind tunnel and by parametric equations derived from experiments(Gullbrekken et al., 2018). It is normally assumed to be independent of wind speed but varies according to wind direction and position on the building surface. It is also significantly affected by neighbouring obstructions (Liddament, 1986). The air density, wind speed, and the shape of the building are taken into account by the wind pressure coefficient in order to determine the wind pressure intensity. The general expression of the wind pressure intensity is therefor given by Equation 2.5:

$$P_w = \frac{1}{2}\rho_{air} C_p v^2 \tag{2.5}$$

where P_w represents wind pressure (Pa), ρ_{air} represents outside air density (kg/m^3), and v represents wind speed (m/s). Typical infiltration and ventilation airflow

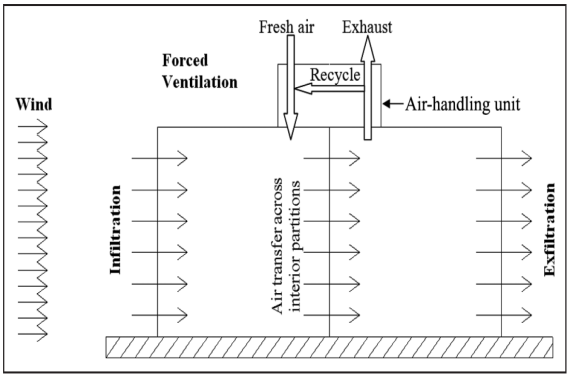

Figure 2.3: Typical infiltration and ventilation airflow (source: Younes et al., 2012)

.

Pressure coefficients are non-dimensional coefficients, and generally calculated from data obtained through parametric equations derived from experiments, wind tunnel, or full-scale tests, on various building shapes and heights (Muehleisen & Patrizi, 2013). In their further analysis, Muehleisen & Patrizi have referred to earlier works of Ginger & Letchford; Ohkuma et al.; Akins; Hussain & Lee to indicate that full-scale and wind-tunnel scale tests are more suited for very complex high-rise buildings or for the development of wind pressure coefficient databases due to level of difficulty, cost and the demand for time and expertise. Parametric equations derived from measurements are rather most commonly used approaches on low-rise buildings for the prediction of C_p.

Liddament asserts that the overall airtightness of the building, and the topographic environment in which the building is located are parameters that can uniquely define the air infiltration characteristics of individual buildings along with the driving mechanisms of infiltration. Liddament argued further for a simultaneous consideration of the primary climatic forces of air infiltration, stating that, *the windiest conditions rarely occur on the coldest days so that taking the extreme values of each parameter separately may result in an overestimate of infiltration.* A graphical representation of this correlation is shown in figure 2.4 as proposed by Liddament.

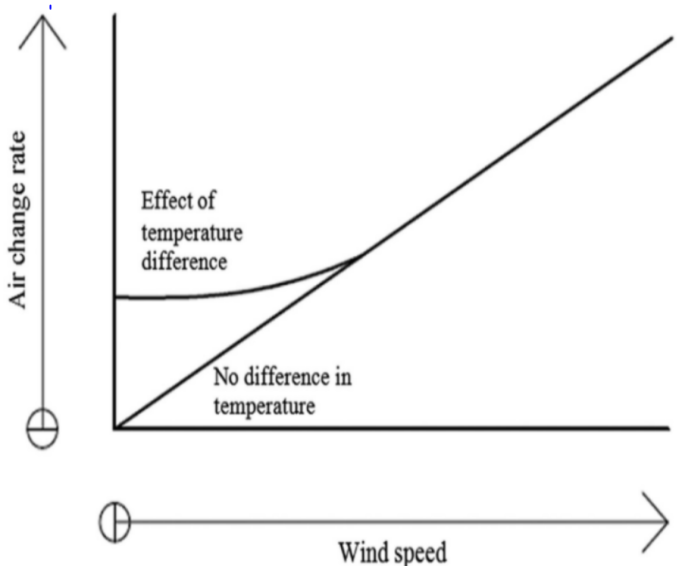

Figure 2.4: Infiltration characteristcs (source: Liddament, 1986)

.

Coincidentally, this proposed correlation was already identified and a 'rule-of-thump' was developed by Shaw (1981), as cited in the work of (Kraniotis, 2014). After conducting a series of experiments, Shaw draw a conclusion stating 'when the temperature difference is less than 20K and the wind speed is greater than 3.5m/s, the wind becomes the dominant driving potential causing infiltration'.

2.2.3 Driving Mechanism: Dynamic Wind

By its nature, atmospheric wind can manifest a turbulence which can result in inducing a corresponding pressure distribution on the building enclosures. The complexity of such fluctuation is increased by the combined effects of terrain roughness and shielding effect arising from surrounding obstacles (Liddament, 1986). Haghighat et al. (2000) heightened the effect of turbulent fluctuation on air infiltration and attributing it not only to the gustiness of the wind but also to the interaction between the wind and the building envelope. Such pressure distribution cannot successfully be represented by the steady state pressure coefficients. In measuring the air tightness of building envelopes, the complex wind fluctuations are disregarded and the prediction of the infiltration rate of the building is based solely on the mean value of input parameters, such as wind velocity, stack effect and mechanical forces (I. S. Walker et al., 1998; Etheridge, 1977).

Experimentally, however, the contribution of pressure fluctuation can be shown under conditions when the mean pressure difference across an opening is small in comparison to the size of the fluctuating component.

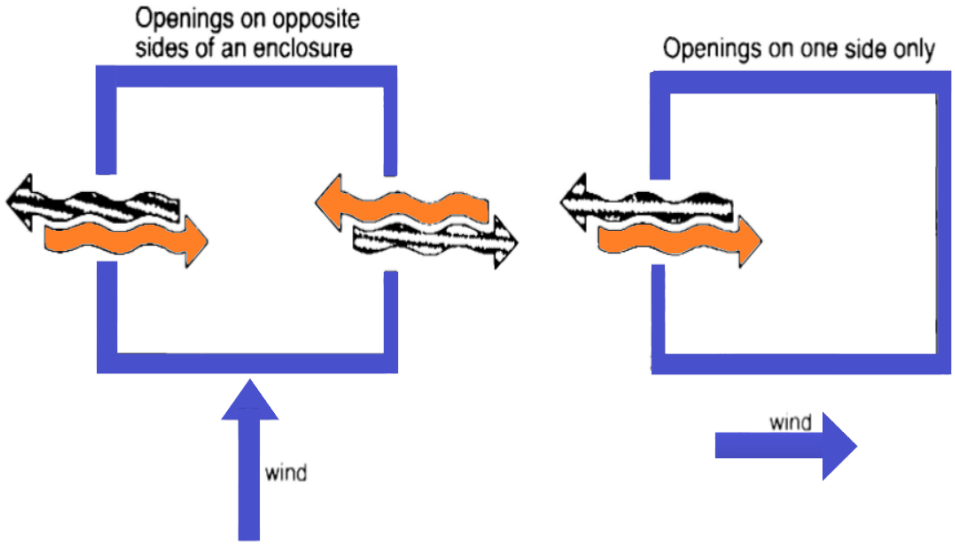

Figure 2.5: Air infiltration due to turbulent fluctuations (source: Liddament, 1986)

.

In determining the wind induced surface pressure (see equation 2.5), the wind velocity at building height becomes the dominating factor as the pressure varies not linearly but with the square of the velocity (Orme et al., 1998). In order to accurately estimate the wind velocity at the building height, an extrapolation analysis on data gathered from a 10 m height meteorological instrumentation is conducted. Such estimation of site wind velocity from meteorological data utilizes wind velocity profile laws and terrain parameters found in table 2.1.

Table 2.1: Meteorological velocity Conversion Parameters

Terrain class	a	Roughness length Z_0	V_{site}/V_{meteo}
Open flat country	0.17	0.03	1.0
Country with scattered wind breaks	0.20	0.25	0.9
Urban	0.25	0.5	0.8
City	0.33	0.5	0.8

With regard to estimating the wind velocity profile, the power law and the logarithmic estimation approaches are discussed below. The power law can only be applied in non-convective conditions, but not in circumstances where the small-scale topography causes local wind accelerations (Orme et al., 1998). The direction of the wind is influenced by the terrain type over which the wind passes over along its path. The terrain roughness parameter therefore becomes vital in accurately estimating the site wind velocity. Consequently any changes in ground height must be gradual for this approach to be valid. The power law is given by

$$\frac{\overline{v}_z}{\overline{v}_\delta} = \left[\frac{Z}{\delta}\right]^a \tag{2.6}$$

where

- z = height above ground (m),

- δ = atmospheric boundary layer thickness (m),
- $\overline{v}_z$ = mean wind velocity at height z (m.s^{-1}),
- $\overline{v}_\delta$ = mean free stream velocity (m.s^{-1}),
- a = roughness parameter dependent on terrain. (See table 2.1)

On the other hand, the logarithmic wind velocity profile is given as follows.

$$\overline{v}_z = \frac{\nu_e}{\kappa} \ln\left[\frac{Z}{Z_0}\right] \tag{2.7}$$

where

- Z = height above ground (m),
- $\overline{v}_z$ = mean wind velocity at height z (m.s^{-1}),
- ν_e = friction velocity (m.s^{-1}) = $\sqrt{\frac{\text{surface drag per unit area}}{\text{density}}}$
- κ = the Karman constant (approximately 0.4),
- Z_0 = the roughness length (m) [1]

The present European standard EN 15242 proposes the logarithmic law approach in estimating the wind velocity profile. Accordingly, the logarithmic law is strictly valid only from 60-100m above ground, but it can be applied for this standard for wind speeds > 2 m/sec and for heights $Z > 20 \cdot Z_0$. Table 2.1 gives the roughness parameter Z_0 at site for the common wind velocity reference height of 10m. However, values for too dense areas cannot be obtained in a similar way, and therefore a displacement height d[2] is employed to introduce a datum ground level at 0.5 ... 0.75 of the height of the obstacles (Orme et al., 1998). The logarithmic profile then becomes

$$\overline{v}_z = \frac{\nu_e}{\kappa} \ln\left[\frac{Z - d}{Z_0}\right] \tag{2.8}$$

This gives a more realistic description of the wind behaviour above the closely spaced obstructions. In order to estimate the mean wind speed at one height (z_2) based on that another (z_1), Equation 2.7 could be rearranged and the logarithmic law is given below by Equation 2.9 as proposed by European standard EN 15242.

$$v(Z_2) = v(Z_1) \frac{\ln(Z_2/Z_0)}{\ln(Z_1/Z_0)} \tag{2.9}$$

2.3 Air Infiltration: Measurement

In deterring the impact of air infiltration, buildings are characterized by a rather intrinsic property referred to as air tightness (Sherman & Chan, 2004). The impact of infiltration on energy efficiency, health effects and construction quality necessitates acquiring an

[1] The height above the displacement plane at which the mean wind becomes zero when extrapolating the logarithmic wind speed profile downward through the surface layer.(American Meteorological Society, 2019)

[2] Zero-plane displacement (d) is the height in meters above the ground at which zero wind speed is achieved as a result of flow obstacles such as trees or buildings(Wikipedia contributors, 2018)

increasing insight on its mechanisms and influence on the air tightness of the building envelope (Leprince et al., 2017).

Air infiltration is highly affected by the air leakage rate (ALR), Q (m^3/s), an important parameter which depends on the pressure difference across the building envelope, ΔP (Pa). The flow resulting from the pressure difference may behave differently at a certain point of a flow field and at a certain time. It may attain a state of laminar, transitional or turbulent flow form. In Equation 2.10 a laminar pressure-flow relationship is represented while Equation 2.11 shows a turbulent flow.

$$Q = K_1 \Delta P \tag{2.10}$$

$$Q = K_2 \Delta P^{\frac{1}{2}} \tag{2.11}$$

where

- Q is the flow rate [m^3/s]
- ΔP is the pressure difference across crack [Pa],
- K_1 is a flow coefficients [m^3/sPa]
- K_2 is a flow coefficients [$m^3/sPa^{\frac{1}{2}}$].

The flow form is further determined by Reynolds number (Re), which relates the velocity of the medium with its dynamic viscosity and the size of the leakage path as in Equation 2.12. It has been found that air flow is fully laminar for Re $<$ 2000 and the flow is normally turbulent for Re $>$ 4000 (Kronvall, 1980). The remaining region that lies between these critical values is the transition region within which the flow alternates between laminar and turbulent with respect to time.

$$Re = \frac{Q \cdot L \cdot \rho}{\mu \cdot A} \tag{2.12}$$

where

- Re is the Reynolds number [-]
- Q is the flow rate [m^3/s]
- L is the hydraulic diameter [m]
- ρ is the density [kg/m^3]
- μ is the dynamic viscosity [Ns/m^2]
- A is the area of the cross section [m^2]

2.3.1 Measurement: Calculating Air Leakage Rate

Air infiltration may take various paths across the building envelopes as in figure 2.7.Thus, a more generalized approach is applied to curb the challenges associated with identifying a specific leakage rout. An illustration of the common leakage sites are also presented in figure 2.6. There are two functional forms proposed in the literature for describing the pressure-flow characteristics across the building envelopes; the power law in Equation 2.13 and the quadratic law in Equation 2.15. The power law assumes that the total air flow is an approximation of flows which follow various leakage paths depending on different

pressure differences. The total flow is considered to be somewhere between laminar and turbulent (Berge, 2011). The quadratic law, on the other hand, is described by combining the limiting cases of laminar and turbulent equation. This pressure-flow relationship still provides inadequate image of the total flow of the actual phenomenon.

$$Q = C\Delta P^{n} \tag{2.13}$$

$$\Delta P = AQ + BQ^2 \tag{2.14}$$

Equation 2.14 can be rearranged so that the flow rate for a known pressure drop is expressed as a quadratic equation;

$$Q = \frac{-A + \sqrt{A^2 + 4B\Delta P}}{2B} \tag{2.15}$$

where

- Q is the flow rate [m^3/s]
- ΔP is the pressure difference [Pa]
- C is the air flow coefficient [$m^3/s\ Pa^n$]
- n is the pressure exponent [-]
- A is the flow coefficient for fully developed laminar friction losses [$(Pa\ s)/m^3$]
- B is the flow coefficient for entry, exit and turbulent flow losses [$(Pa\ s^2)/m^6$]

The air flow exponent (n) is an indication of the type of leaks that dominates the building. It shall be in the range 0.5 to 1, but often set to 0.7 in the equation $C\Delta P^n$ for the regression curve. A very sharp deviation from 0.7 is considered an indication of the leaks that dominate the building. Large openings and holes give a low exponent, narrow cracks or leakage through materials gives high exponent. It can also be affected by the wind situation, loss temporary seals, or other errors in the measurement situation can affect the exponent n (Tormod Aurlien, 2014). The air flow coefficient C denotes the amount of air leaking into the building.

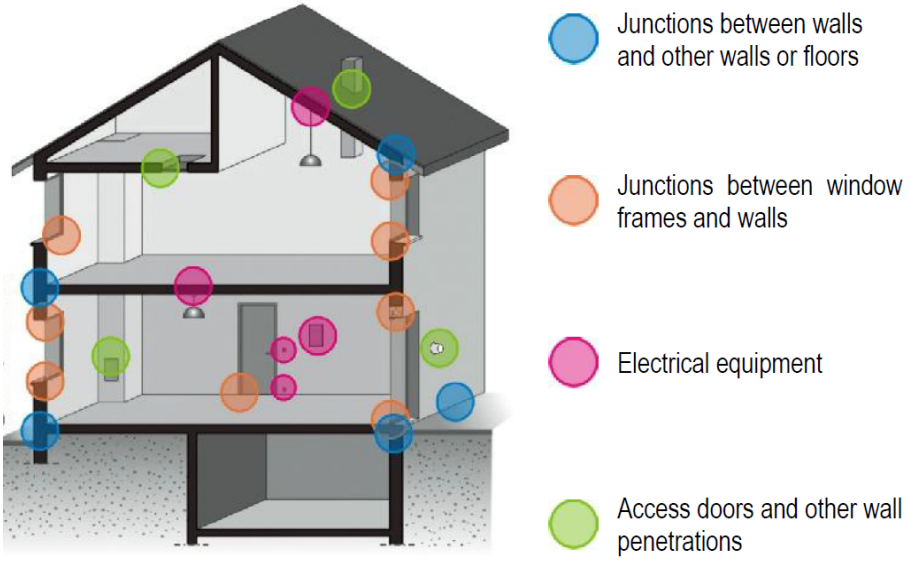

Figure 2.6: Common leakage sites classified in 4 categories (source: Carrié et al., 2012)

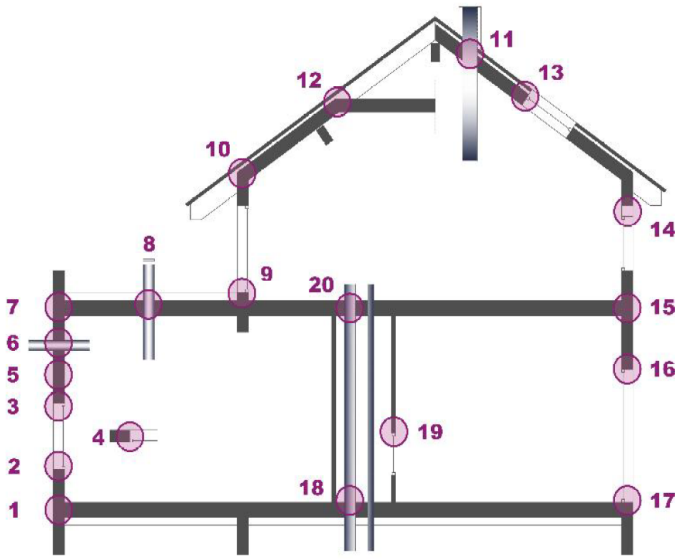

Figure 2.7: Vertical section of a typical building with identification of potential leakage junctions (source: Carrié et al., 2012)

1. Junction lower floor / vertical wall
2. Junction window sill / vertical wall
3. Junction window lintel / vertical wall
4. Junction window reveal / vertical wall (horizontal view)
5. Vertical wall (Cross section)
6. Perforation vertical wall
7. Junction top floor / vertical wall
8. Penetration of top floor
9. Junction French window / vertical wall
10. Junction inclined roof / vertical wall
11. Penetration inclined roof
12. Junction inclined roof / roof ridge
13. Junction inclined roof / window
14. Junction rolling blind / vertical wall
15. Junction intermediate floor / vertical wall
16. Junction exterior door lintel / vertical wall
17. Junction exterior door sill / sill
18. Penetration lower floor / crawlspace or basement
19. Junction service shaft / access door
20. Junction internal wall / intermediate floor

The pressure-flow relationships stated in equations 2.13 and 2.15 has raised questions concerning their description of the true natural conditions, i.e. ventilation condition. The fact that natural ventilation conditions (air infiltrations) take place at a lower pressure differences across the skin of the building, necessitates extrapolation of data measured at high pressure differences down to the actual pressure. Thereby suggesting the relevance of the extrapolation approach being employed. A study conducted by I. Walker et al. (1996) proposed that "*the power law can give a close representation of an equation which is analytic solution of the basic equations of motions* ". A counter argument was proposed by (Etheridge, 1998) showing that the power law fails to adequately model the behaviour of adventitious openings at low pressure differences by up to 40 percent or more in comparison to the quadratic law.

Following this criticism, I. S. Walker et al. (1998) used theoretical approach combined with laboratory and field measurements to examine the validity of the power law and concluded its validity for low pressure building envelope leakage. However, a recent publication based on a CFD (Computational Fluid Dynamics) approach has emerged in favour of the quadratic law (Chiu & Etheridge, 2002). Despite these disparities concerning which approach describes the true natural condition of pressure-flow relationship, the European and other well practiced standards and calculation procedures use the power law function to extrapolate from data measured at high pressure differences down to the pressures experienced by the building envelope for natural infiltration (CEN, 2015; ASTM International, 2019).

2.3.2 Measurement Techniques: Quantifying Air Infiltration/Leakge Rate

Various techniques have been developed and applied to measure airflow across building enclosures. The tracer gas method, fan pressurization, AC pressurization, infrasonic impedance, acoustic techniques, and quantified thermography are such techniques mentioned in the review work of J. McWilliams (J. McWilliams, 2002). Among these measurement techniques, fan pressurization is the most widely used technique proposed by NS-EN ISO 9972:2015 and in quantifying the thermal performance of buildings.

The fan pressurization method measures envelope leakage by either a single measurement of fan flow needed to create a 50 Pascal change in building pressure, or by establishing a range of pressure differences in increments of no more that approximately 10 Pascal. Conventionally, a single point test performed at the 50 Pa pressure difference would be determinant in the measurement of Air Leakage Rate, Q (m^3/s) (Vega Pasos et al., 2019). The range of induced pressure differences are the bases for multiple point test fitting the curve of the Equation 2.13. The One-Point Test procedure have the advantage of providing a quick and simple building airtightness analysis. On the other hand, making multiple measurements increases test accuracy by averaging out errors due to fluctuating pressures and operator. The leakage area of the building (i.e. the cumulative size of the hole in the building envelope) can also be estimated based on the Multi-Point Test (The Energy Conservatory, 2007a).

Often the pressure across the envelope is susceptible to varying wind and weather conditions, which correspondingly influences the flow across the enclosure when performing the fan pressurization test. To take this into account and reduce its influence, the induced pressure-offset is deducted from the actually measured pressure differences. The International Standard NS-EN ISO9972:2015(E) refers to this induced pressure offset as the zero-flow pressure difference, and is normally measured before and after the actual pressurization test.

2.4 Uncertainty of Measurement Techniques

The purpose of conducting the fan pressurization test is to measure the air flow through the enclosure. Yet, it neither provides a direct measurement of the air infiltration rate nor the heat load. A direct measurement of the air infiltration rate may however be conducted by other approaches, like tracer gas methods. The estimation procedure involves derived quantities such as the air flow coefficient, C, and the pressure exponent, n, described in Equation 2.13. Although such procedures are part of a standard protocol, it is observed (Carrie & Wouters, 2012) that differences in the derived quantities may arise depending on the test and on the tester. The International Standard NS-EN ISO9972:2015(E) takes into account estimation of the uncertainty associated with the derived quantities of C and n and suggests a procedure for estimating the uncertainty as well as its inclusion in

the data analysis. It should be noted that this uncertainty is not the uncertainty of the measurement it self but rather of the derived quantities. According to the report by Carrie & Wouters, the sources of uncertainty in derived quantities may include the following.

- The building preparation-i.e., the conditions of intentional openings and natural ventilation in the measurement. By condition we mean either being closed, sealed or open depending on the test method selected and the purpose of the test.
- Reference values such as envelope area and net floor area are calculated according to national regulations, the internal volume remains subject to interpretations.
- Sampling assumptions may based on the size of the buildings (multi-family vs single family/semi-detached houses). Practical constraints and economical feasibility influence the course of an airtightness test
- The equipment uncertainty and software errors. Deviation between test results may arise due to insufficient calibration of pressure and flow measurement devices, particularly when performing measurement of low flow rates.
- The influence of wind and temperature, as discussed in earlier sections, play an important role in building infiltration and in calculating the air flow rate, reference pressure, data collection protocol and analysis method.

Chapter 3

Methods

3.1 Experimental Site

The experimental data required to complete this master thesis were obtained from measurements conducted at the meteorological field station of the Norwegian University of Life Science (NMBU) in Ås, Norway (59.66°N / 10.78°E). The field station for bio-climatic studies is a fully automated field laboratory, equipped with extensive logging and measuring equipment for 24-hour continuous records of meteorological observations, radiation measurement, soil temperature profiles and more from over 50 instruments.The field station covers 12 acres and is located in the center of ca 500 acres relatively flat landscape (se figure 3.1a). It is surrounded by woods and villas with a minimum distance of 200m, rendering it an open terrain classification.

(a) The Field Station for Bio-Climatic Studies

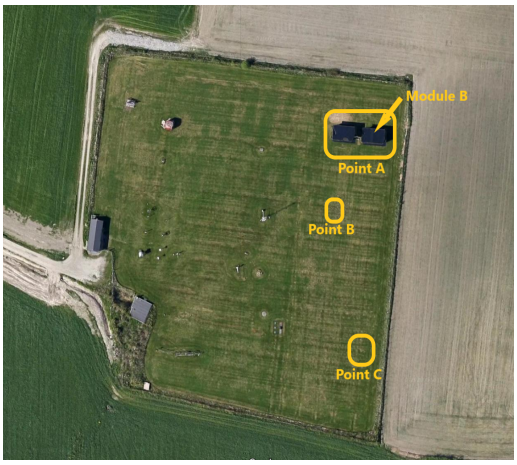

(b) Point A: Test Room, Point B: Anemometer Location and Point C: Solar Panel Structure

Figure 3.1: Overview of the Meteorological Field of NMBU and its surroundings (Source: (Google Maps, 2020))

For the purposes of fan pressurization measurements and installation of anemometer instrument, the two respective positions (Point A and Point B) marked in figure 3.1b were consistently used. The initial plan of positioning the anemometer from the south facade of the building module A, was altered due to the presence of solar panel structure at Point C as depicted in figure 3.1b.

3.2 Test Room

The basic dimensions for the test-room and the corresponding building reference values applied in the pressurization test are given respectively in table 3.1 and 3.2. The data obtained from the original drawings (se appendix A) informs the thermal performance of the enclosure where the design u-value of the different building parts are given as follows; Ceiling/Roof: $1.5\left[\frac{W}{m^2K}\right]$, Floor: $1.29\left[\frac{W}{m^2K}\right]$, and External Wall: $0.31\left[\frac{W}{m^2K}\right]$.

Table 3.1: The Basic Test-room Dimensions

	Internal Dimensions	External Dimensions
Length [m]	7 m	7.4 m
Width [m]	3.6 m	4.05 m
Height [m]	2.26 m	2.65 m
Elevation [AMSL [1]] [m]	90 m	

Table 3.2: Building Reference Value

Internal Volume [m^3]	56.952 [m^3]
Net Floor Area [m^2]	25.2 [m^2]
Envelope Area [m^2]	60.685 [m^2]

The floor plan of the test rooms in figure 3.2 illustrate the relative geographical position of the building with respect to the north pole. The southern facade is orthogonal in its orientation to the wind blowing from the south, with two window installed in the building envelope. The test is proposed to be conducted in module B, with its door facing towards the west direction. Module A stands in a close proximity of about 2.5m.

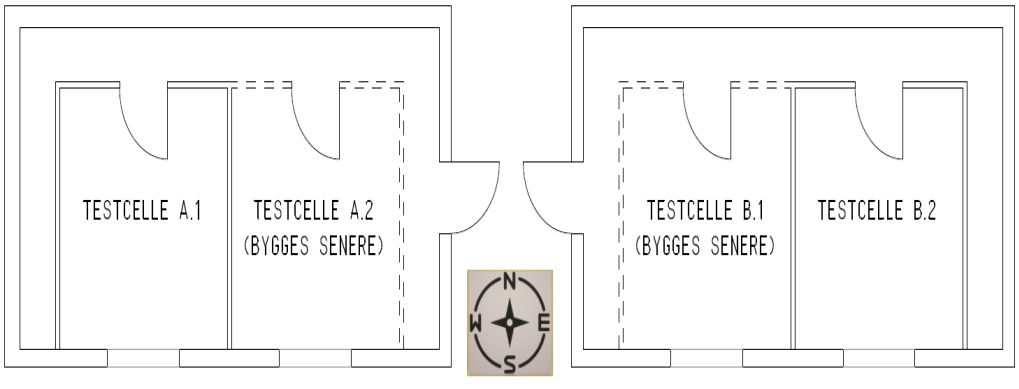

Figure 3.2: Relative position of Test room: Floor Plan of Module A and B

3.3 Blower Door Test

3.3.1 Instrument

A Minneapolis Blower Door system is used to measure the building pressures across the envelope. It is comprised of three separate components: 1) Blower Door Fan, 2) Building pressure and fan flow gauges, Fan Speed Controller and Nylon Door Panel and 3)The Adjustable Aluminum Door Frame. A digital pressure gauge known as DG-700, was used

Figure 3.3: Blower door under operation.

in automating the measurement, documentation and analysis of the Blower Door test results along with TECTITE software. A picture demonstrating the blower door from the test room is presented in Figure 3.3.

In order to measure air flow during a Blower Door test, air must flow through the fan inlet and out the exhaust side of the fan (The Energy Conservatory, 2007a). A practical challenge was to keep the direction of the Blower Door fan flow consistent with an indicated mode of test. An automatic alteration of air flow direction wasn't possible on the fan model 4 used in this study, requiring the operator to engage physically and reverse the fan to achieve a correct flow direction with respect to the mode of the test (i.e. depressurization vs. pressurization). Furthermore, the necessary adjustments were made to the factory settings pertaining to the target pressures and test parameters while performing the test mostly at the request of TECTITE software. The parameters supplied for the automated testing and the corresponding adjustments are presented in table 3.3.

Table 3.3: Test Parameters

	Factory Test Settings	Actual Test Settings
Samples per station	200	Not Changed
Fan Adjust Rate	1.0	Not Changed
Target Tolerance [Pa]	2Pa	2Pa\5Pa\10Pa
Building High Pressure Limit [Pa]	90Pa	100Pa
Fan Start [%]	0.0	Not Changed

The air flow capacity of the Blower Door fan can be configured by installing the Flow Rings on the fan inlet. The Flow Rings have 6 different flow capacities (se table 3.4) of which only the highlighted 4 configurations were available for this particular study.

Table 3.4: Fan Flow Range

Fan Configuration	Flow Range (cfm) for Model 4 Fan
Open (no Flow Ring)	4800 - 2090
Ring A	2500 - 790
Ring B	900 - 240
Ring C	260 - 45
Ring D	125 - 30
Ring E	50 - 11

3.3.2 Procedures

The Blower Door Test procedure involved testing the building over a range of target pressures. Such approach is also known as a Multi-Point Test. Usually, blower door measurements are taken at high pressures because these measurements are highly repeatable and are less subject to large variations due to changes in wind speed and direction (The Energy Conservatory, 2007a). This was also highlighted in the NS-EN ISO 9972:2015 standard where readings up to 100 Pascal are recommended for a more accurate calculated results. However, for the purpose of this particular study, target pressures supplied as a default values (Se table3.5) in the TECTITE software were applied.

Table 3.5: Target Pressure from TECTITE Software

#1	#2	#3	#4	#5	#6	#7	#8	#9	#10
64Pa	58Pa	52Pa	48Pa	40Pa	34Pa	28Pa	22Pa	16Pa	10Pa

Generally, the measurements were taken in a course of ten days, where a set of eight pressurization tests were followed by another set of eight depressurization tests or vise versa on each day. The testes are basically designated by numbers ranging from 1 to 10, with an exception of the test performed on Day 1. The blower door test on Day 1 was additionally marked with alphabets, such that the tests are designated by a test number followed by an alphabet, "A" or "B".

The alphabetical specification differentiate between two types of air leakage rate graphs obtained during Day 1. Test results designated by "A" represent the first type of air leakage rate graph constituting two depressurization and one pressurization measurement. The second type of air leakage rate graph is designated by alphabet "B" and comprises two independent graphs, where the first graph depicts results from eight pressurization tests, and the second graph depict four depressurization measurements reported separately[2].

[2]For further clarity, refer to table 4.6 for Day 1. The top middle plot is designated by "A" and the bottom two plots are designated by "B".

3.4 Wind Measurements

3.4.1 Instrument

The wind data of dynamic condition was captured by an ultrasonic anemometer device, Model: 1590- PK- 020, that can perform measurements in wind speeds up to 45 m/s(Se Figure 3.4). It was mounted at the height of 2.2m above the ground on the meteorological field site, from the south facade of the building module A. It was located at a distance of 20m without any obstruction within a radius of ca 18m. The wind master anemometer measures the times taken for an ultrasonic pulse of sound to travel from an upper transducer to the opposite lower transducer, and compares it with the time for a pulse to travel from lower to upper transducer (Gill Instruments, 2010). It provides three-axis wind measurement at 20Hz data sampling rate for the purpose of this study.

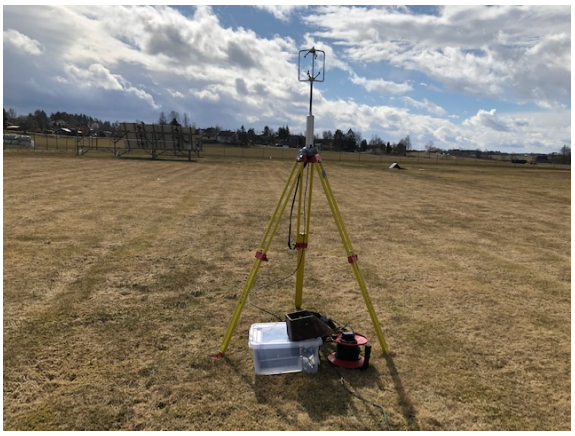

Figure 3.4: Ultrasonic anemometer under operation.

The meteorological wind data is provided by the onsite Field Station for Bio-climatic Studies - BIOKLIM, at NMBU on the Søråas field in Ås. It is the absolute value of the wind speed in the horizontal plane at a height of 10 m. The raw data was acquired at a frequency of 0.1 Hz, i.e one sample every ten seconds, averaged over 10 minutes (Redaksjonen, 2019). It should however be noted that these mean speeds do not capture the speed of wind gusts. An average wind speed from an hourly compiled data is processed further to be utilized making it a basis for this study.

3.4.2 Procedures

The wind conditions during the test can be qualitatively described by its wind class(The Energy Conservatory, 2007b). The Beaufort Scale for classification of wind force is used for such qualitative description, and is presented in Annex D of the ISO 9972: 2015 Standard, Table D.1 . A partial extract of the Beaufort scale relevant for the observed measurements in this study is presented in table 3.6 below.

Table 3.6: Beaufort scale for classification of wind force

Beaufort wind force term	speed equivalent at a standard height of 10 m above open flat ground	Specifications at Land area
Calm	0 to 0.2 m/s	Smoke rises vertically
Light Air	0.3 to 1.5 m/s	Direction of wind shown by smoke but not by wind vanes
Light Breeze	1.6 to 3.3 m/s	Wind felt on face; leaves rustle; ordinary vane moved by wind
Gentle Breeze	3.4 to 5.4 m/s	Leaves and small twigs in constant motion; wind extends light flag
Moderate Breeze	5.5 to 7.9 m/s	Raises dust and loose paper; small branches are moved
Fresh Breeze	8.0 to 10.7 m/s	Ssmall trees in leaf begin to sway; crested wavelets form on inland waters
Strong Breeze	10.8 to 13.8 m/s	Large branches in motion; telegraph wires whistle; umbrellas used with difficulty
Moderate Gale	13.9 to 17.1 m/s	Whole trees in motion; inconvenience in walking against wind
Fresh Gale	17.2 to 20.7 m/s	Breaks twigs off trees; generally impedes progress
Strong Gale	20.8 to 24.4 m/s	Slight structural; damage occurs (chimney pots and slates removed)

3.5 Statistical Modelling and Wind Signal Analysis

3.5.1 Confidence Interval (CI)

A confidence interval is a way of specifying error margins for a measurement or calculation. It specifies the interval with in which an average of measurement population can be predicted by a 95% probability. When calculating the confidence interval, the t-test (Student's test) is used. A t-test is a parametric test type which assumes a signal distribution that is Gaussian in nature. A t-test is used to compare two small samples to see if there is a significant difference. Nonetheless, it may also be applied for sample sizes that are large, usually over 20 times. The confidence interval is calculated based on the procedures in Annex C in ISO 9972 for wind speed magnitude, V_{xy}. An estimate of the confidence interval requires determination of the central tendency (i.e. mean value in Equation 3.1) and dispersion character (i.e. standard deviation in Equation 3.2) (Trochim, 2020).

$$\overline{V}_{xy} = \frac{1}{N}\sum_{i=1}^{N} V_{xy_i} \tag{3.1}$$

$$\sigma = \sqrt{\frac{1}{N}\sum_{i=1}^{N}(V_{xy_i} - \overline{V}_{xy})} \tag{3.2}$$

If T(P,N) is the confidence limit of the two-sided student's t distribution for a probability P on N events, the mean wind measurement lies in the confidence interval as in Equation 3.3,

$$\left[\overline{V}_{xy} - \sigma, \quad \overline{V}_{xy} + \sigma\right] \tag{3.3}$$

3.5.2 Probability Density Function (PDF)

A probability density function is a function that provides the likelihood of obtaining the value assumed by a random variable based on the underlying probability distribution. Analyzing the distribution characteristics requires an effective approach that enables a comprehensive description of the overall situation of the data. The literature on wind speed, wind direction and wind probability distribution offers a range of pdf models (Luis, 2015; Chadee & Sharma, 2001; Morgan, 1995; B. McWilliams et al., 1979; Mazzeo et al., 2018). Accordingly, the probability distribution of wind speed is commonly assumed to be a member of the Weibull family of distribution. When the lower bound is zero, the Weibull pdf is given by

$$f(V_{\mathrm{xy}}) = \frac{k}{c}\left(\frac{V_{\mathrm{xy}}}{c}\right)^{k-1} exp\left[-\left(\frac{V_{\mathrm{xy}}}{c}^{k}\right)\right] \tag{3.4}$$

where $f(V_{\mathrm{xy}})$ is the probability of observing wind speed V_{xy}, c is scale parameter in units of wind speed, and k the dimensionless shape parameter. Once these parameters are estimated at one height, Weibull distribution makes it possible to adjust these parameters to different heights (Akdağ & Dinler, 2009).

There are several methods to estimate Weibull parameters. (Akdağ & Dinler, 2009) mention the commonly used parameter estimators such as Graphic Method, Maximum Likelihood Method MLM) and Moment Method (MM). The MATLAB@ programming software applied in this study uses the Maximum Likelihood Method (MATLAB, 2020b). The shape and scalar parameters can be computed from Equations 3.5 and 3.6 given by

$$k = \left(\frac{\sum_{i=1}^{n} V_{\mathrm{xy_i}}{}^{k} ln(V_{\mathrm{xy_i}})}{\sum_{i=1}^{n} V_{\mathrm{xy_i}}{}^{k}} - \frac{\sum_{i=1}^{n} ln(V_{\mathrm{xy_i}})}{n}\right)^{-1} \tag{3.5}$$

$$c = \left(\frac{\sum_{i=1}^{n} (V_{\mathrm{xy_i}})^{k}}{n}\right)^{-1} \tag{3.6}$$

where $\mathrm{V_{xy_i}}$ is the wind speed and n is the number of nonzero wind speeds.

Wind energy estimation may also be conducted based on Weibull parameters and two significant wind speeds. These two wind speeds are the most probable wind speed and the wind speed carrying maximum energy and are expressed by Equation 3.7 and 3.8. The most probable wind speed ($V_{\mathrm{xy}_{pdf}}$) is the most frequent wind speed for a given wind probability distribution and corresponds to the peak of the probability density function (Oyedepo et al., 2012). It is expressed by,

$$V_{\mathrm{xy}_{pdf}} = c\left(\frac{k-1}{k}\right)^{\frac{1}{k}} \tag{3.7}$$

The wind speed carrying maximum energy ($V_{\mathrm{xy}_{MaxE}}$) identifies the wind speed that carries the maximum amount of wind energy. It is expressed as follows

$$V_{\mathrm{xy}_{MaxE}} = c\left(\frac{k+2}{k}\right)^{\frac{1}{k}} \tag{3.8}$$

The weibull distribution neglects the effect of the direction of the wind (Morgan, 1995; B. McWilliams et al., 1979). B. McWilliams et al. assumed that "the components of the wind velocity in the direction of the prevailing wind and that in the transverse direction are each normally distributed". According to Morgan, when the shape parameter of Weibull distribution is k = 3.5, one may approximate the normal or Gaussian probability distribution.

A brief summary of the normal distribution is follow. The normal or Gaussian probability distribution in Equation 3.9 is also a two-parameter family of curves. the Two parameters are the mean wind speed and standard deviation. It's built upon the Central Limit theorem, which states that the sum of independent samples from any distribution with finite mean and variance converges to the normal distribution as the sample size goes to infinity(MATLAB, 2020a). For the purpose of this study, a Weibull probability density

function of is applied.

$$f(V_{xy}, \overline{V}_{xy}, \sigma) = \frac{1}{\sqrt{2\pi}\sigma} exp\left[-\frac{1}{2}\left(\frac{V_{xy} - \overline{V}_{xy}}{\sigma}\right)^2\right] \tag{3.9}$$

where is the σ standard deviation, and $-\infty < V_{xy} < \infty, -\infty < \overline{V}_{xy} < \infty$ and $\sigma > 0$. The Normal or Gaussian wind speed distribution is also calculated for comparison of under- or overestimation. Similar estimation of wind direction will not be conducted as part of this study.

3.5.3 Spectral Density Estimation (SDE)

The essence of the spectral density estimation is to estimate the spectral density (also known as the power spectral density) of a random signal from a sequence of time samples of the signal (Stoica et al., 2005). It is a process that quantifies the various amounts (e.g. amplitudes, powers, intensities) versus frequency (or phase). It requires a transformation of the wind signal series in time domain to the frequency domain using the fast Fourier transform (FFT) algorithm as defined by Equation 3.10 (Newland, 2012).

$$V_{xy}{}'(k) = \sum_{t=0}^{N-1} V_{xy}(n) e^{\frac{-j2\pi nk}{N}} \tag{3.10}$$

where:

- $V_{xy}{}'$ = the frequency domain representation of the wind fluctuations of the speed i the X-Y axis,
- k = the k^{th} frequency component,
- n = the n^{th} sample (in the time domain,
- N = the total number of samples of V_{xy},
- j = the imaginary unit.

Power spectral density (PSD) can be estimated by computing the magnitude squared of its DFT as defined in Equation 3.11. Such estimation from the frequency domain provides information about the power of each frequency component.

$$S(\omega) = \left|V_{xy}{}'(k)\right|^2 \tag{3.11}$$

The spectrum analysis can be instrumental in identifying the frequencies that carry the signal power or signal energy. In order to achieve this, one may implement various signal smoothing techniques which usually reduces the noise in a signal. Smoothing can help identify trends in signals without distorting them immensely. It aims at removing rough, fast changing components in the signal, and highlight slow changes in value so that it is easier to observe trends in the data.

Different filters are available to perform signal smoothing including, moving average filter (for instance, sliding-average, triangular and pseudo-Gaussian) and savitzky-golay filter (O'Haver, 2019). The Savitzky-Golay smooth has shown to preserve the shape of the original signal with the smallest peak distortion. On the other hand, if the purpose of smoothing is to reduce the noise in the signal and not focus on the retention of the shape of the signal, the triangular or pseudo-Gaussian smooth is suited to this purpose with an additional advantage of faster computation speed. Taking into account computational

speed and risk of signal distortion, the Sliding-average smooth function is selected as a compromise for further implementation in this study. The ready-made Sliding-average smooth function used here is developed by O'Haver.

Chapter 4

Results and Analysis

The impact of variation in wind speed and direction on the Air Leakage Rate (ALR) during the fan pressurization testing was assessed based on the evaluation of a total 158 Blower door tests. Amongst of which 80 were pressurization tests and 78 were depressurization tests.

4.1 Measurement conditions

4.1.1 Temperature

Indoor temperature in the test room before, during and after the blower door measurement is read from a thermometer of room heater, which was set to 21°C for the whole period of the test. Data for the outdoor temperature was retrieved from the onsite Field Station for Bio-climatic Studies - BIOKLIM, at NMBU on the Sørås field in Ås. The mean temperatures calculated for the hours during the test on each day reveals a temperature variation with interval approximating from 4°C to 20°C. The effect of indoor/outdoor temperature difference on the Air Leakage Rate (q_{50}) is suggested to be neglected for wind cases greater than 3.5 m/s on a condition that the temperature difference across the building enclosure remains under 20 K (Shaw, 1981).

Parallally, the standard, NS-EN ISO 9972:2015 proposes that if the product of the indoor/outdoor air temperature difference, expressed in Kelvin, multiplied by the height of the building, expressed in metres, gives a result greater that 250 mK, it is unlikely that a satisfactory zero-flow pressure difference can be obtained. The proposition from the later case is presented in table 4.1, and accordingly should the zero-flow pressure differences for all measurements be satisfied. Interestingly, this was not the case owning to a predominantly windy conditions incurred, of which the effect will be discussed in later sections. The effect of indoor/outdoor temperature differences were consequently considered minimal therefore disregarded for the purpose of this study.

4.1.2 Wind

A range of varying wind conditions were registered throughout the testing period. Accordingly, a wind class ranging from [Wind Force Level 2: Light breeze] to [Wind Force Level 5: Fresh breeze] in the Beaufort wind force scale is observed during the test period. An overview of the different wind classes and their respective values are presented in table 4.2 and 4.3.

ISO 9972 states that a wind speed near the ground that exceeds 3 m/s or a meteorological wind speed above 6 m/s or a wind force that reaches level 3 on the Beaufort scale, is unlikely to satisfy the zero-flow pressure difference requirement. Combined with the

Table 4.1: Indoor/outdoor Air Temperature Difference

	Indoor Temperature [°C]	Outdoor Temperature [°C]	Temperature Difference [mK]
Day 1	21	4.8	35.6
Day 2	21	6.5	32.0
Day 3	21	6.6	31.7
Day 4	21	10.0	24.2
Day 5	21	5.0	35.3
Day 6	21	13.0	17.6
Day 7	21	9.7	24.9
Day 8	21	5.9	33.2
Day 9	21	16.5	9.8
Day 10	21	19.7	2.9

remarks of Shaw presented in the previous subsection, the following observation is noted. Upon inspection of the results in table 4.2 and 4.3, only measurements from Day 2, Day 4, Day 6, Day 7, Day 8 and Day 10 are within the meteorological wind speed limit. The corresponding wind speed measurements at the building's height[1] however were not under the recommended wind speed limit of 3 m/s. Thus, valid zero-pressure difference measurements may be attainable for Day 7, Day 8 and Day 10 in both pressurization and depressurization modes of measurements.

[1]It is defined to be equivalent to the wind speed near the ground for the purpose of this study (Zheng et al., 2019)

Table 4.2: Summary of Pressurization Test Results at 50 Pascals

	Test Results at 50 Pascals:			Building Leakage Curve:				Wind Condition:			
Day #	Air Leakage Rate: q_{50} $[\frac{m^3}{h}]$	Leakage Areas:ELA_{50} $[m^2]$	Air Flow Coefficient C_{env}	Air Leakage Coefficient C_L	Air Flow Exponent n	Determination Coefficient: $[r^2]$	Wind Class	Wind Direction	Mean Wind Speed Magnitude at 2.2m $[\frac{m}{s}]$	Meteorological Wind Speed at 10m $[\frac{m}{s}]$
1A	283	0.0086	31.6	31.5	0.561	0.93828	Fresh breeze	SSE	7.01	9.13
1B	269	0.0082	34.9	34.9	0.522	0.89903	Fresh breeze	SSW	7.55	9.56
2	279	0.0085	18	18	0.701	0.98515	Gentle breeze	SSE	4.03	4.68
3	278	0.0085	17.1	17.1	0.713	0.99151	Moderate breeze	NNW	4.33	6.17
4	289	0.0088	16.9	16.9	0.726	0.98968	Gentle breeze	WWN	4.82	3.22
5	304	0.0093	16.6	16.6	0.744	0.82193	Fresh breeze	WWS	7.15	8.45
6	314	0.0096	18.2	18.2	0.728	0.99471	Gentle breeze	WWS	3.55	2.89
7	313	0.0095	19.3	19.3	0.712	0.98242	Light breeze	NW	2.32	2.58
8	311	0.0095	17.4	17.3	0.738	0.99511	Gentle breeze	SW	2.92	4.12
9	313	0.0095	16.4	16.4	0.754	0.97962	Moderate breeze	SSW	5.90	7.47
10	302	0.0092	15.9	15.9	0.753	0.99566	Light breeze	WWN	2.24	2.84

Table 4.3: Summary of Depressurization Test Results at 50 Pascals

	Test Results at 50 Pascals:			Building Leakage Curve:				Wind Condition:			
Day #	Air Leakage Rate: q_{50} $[\frac{m^3}{h}]$	Leakage Areas:ELA_{50} $[m^2]$	Air Flow Coefficient C_{env}	Air Leakage Coefficient C_L	Air Flow Exponent n	Determination Coefficient: $[r^2]$	Wind Class	Wind Direction	Mean Wind Magnitude at 2.2m $[\frac{m}{s}]$	Meteorological Wind Speed at 10m $[\frac{m}{s}]$
1A	191	0.0058	17.5	17.9	0.606	0.97508	Fresh breeze	SSW	7.56	9.08
1B	186	0.0057	13.4	13.6	0.667	0.93826	Fresh breeze	SSW	7.02	8.72
2	184	0.0056	11.3	11.4	0.711	0.98592	Gentle breeze	SSE	4.78	5.96
3	183	0.0056	10.1	10.2	0.738	0.99557	Moderate breeze	NNE	4.31	6.86
4	186	0.0057	8.9	8.9	0.775	0.97915	Gentle breeze	WWN	5.29	5.65
5	198	0.0060	7.6	7.7	0.831	0.97466	Fresh breeze	WWS	7.55	8.09
6	212	0.0065	10.2	10.3	0.774	0.99282	Gentle breeze	WWN	3.67	4.46
7	225	0.0069	12	12.1	0.746	0.99563	Light breeze	WWN	2.34	2.71
8	204	0.0062	10.4	10.5	0.758	0.99817	Gentle breeze	WWS	1.63	3.34
9	209	0.0064	12.7	12.7	0.715	0.96174	Moderate breeze	SSW	6.07	5.80
10	208	0.0063	10.4	10.4	0.766	0.99871	Light breeze	WWN	1.72	2.25

4.2 Air Leakage Rate (ALR - q_{50})

The Blower-door test considers the establishment of a valid Zero-flow pressure difference a requirement in qualifying the outcomes of the two modes of measurements. The measurement conditions discussed i section 4.1 are complemented by the following criteria in identifying the Air Leakage Rate across the envelope.

The table is coded in such a manner that the individual tests from each mode of measurements are evaluated against the five criteria listed blow.

- air flow exponent (n): $0.5 \leq n \leq 1$
- coefficient of determination (r^2): $0.98 \leq r^2 \leq 1$
- zero-flow pressure difference (baseline pressure value):

$$\left\{ \begin{array}{l} |\Delta p01+| \text{ and } |\Delta p01-| \\ |\Delta p02+| \text{ and } |\Delta p02-| \end{array} \right\} \leq 5Pa$$

- pressure difference sequence (ΔP): $\Delta P \leq 10Pa$
- lowest target pressure difference (ΔP):

$$\Delta P = \left\{ \begin{array}{ll} 10\ 3\,\%Pa, & \text{if } [10\ 3\,\% \geq 5 * \Delta p01] \\ 5 * \Delta p01, & \text{if } [5 * \Delta p01 \geq 10\ 3\,\%] \end{array} \right\}$$

The test results are marked either "Green" or "Red" indicating whether a criterion is satisfied in the former case or not satisfied in the later one. In cases where a partial compliancy is observed, the "Red" marker is applied to indicate those only not satisfied while the remaining lots are left unmarked.

4.2.1 Criteria Analysis

A full summary of all relevant criteria along with corresponding deviations from the recommended reference values in ISO 9972 is presented in table 4.5.Thus, allowing an assessment of table 4.2 and table 4.3 for eligibility identification and further analysis.

An assessment of compliancy for all criteria mentioned above qualifies only pressurization mode of measurements of Day 6 and Day 10. The wind situation under which the tests were conducted for these two days, however, reveals different wind conditions. A mean wind speed of 3.55 m/s and 2.24 m/s at the height of the building was reported respectively for Day 6 and Day 10. Although the recommended meteorological wind speed limit (6 m/s) and Beaufort scale [Wind Force Level 3: Gentle breeze] were not exceeded in both cases, only the mean wind speed at the building height for Day 10 was below standard limit of 3 m/s.

It should also be noted from the pressurization mode of measurements, the likelihood of achieving a satisfactory zero-pressure difference is not guaranteed despite being reported a favorable wind condition, as it appears on Day 7 and day 8. One may also observe partially valid wind speed compliancy as it occurs on Day 2, Day 3 and Day 4. The term partial validity is used here to give emphasis on occurrence of acceptable outcomes which are independent of one another. In another word, an acceptable meteorological wind speed limit does not mean the requirement for wind speed limit at the height of building

is satisfied or vice versa. Moving forward, the ALR from Day 10, equivalent to 302 $[\frac{m^3}{h}]$ is considered as a reference value for the pressurization mode of measurements.

The depressurization mode of measurement, on the other hand, fails to meet the requirements set by the standard despite a favorable wind conditions registered on days such as Day 7, Day 8 and Day 10. The wind speeds from Day 2, Day 3 and Day 6 are considered partially valid[2].

For the purpose of this study, an ALR value that represent the mode of measurement was assumed based on a comparison of deviations registered on days with favorable wind condition. The deviation report on Day 7 exhibits deviation on one of the criteria, among which one valid outcome is observed on the fourth test of the day. While the measurements on Day 8 indicate two sources of invalid criteria, only one source of invalid criteria is registered for Day 10. In an absence of a clearly identified reference value, the ALR determined by the depressurization test, equivalent to 225 $[\frac{m^3}{h}]$ is assumed to approximate for the study presented hereafter.

Table 4.4: Reference Values for Pressurization and Depressurization Mode of Measurements

Reference Mode of Measurement	Air Leakage Rate	Air Leakage Coefficient	Air Flow Exponent	Determination Coefficient	Wind Speed At Building Height	Wind Speed At 10m	Wind Direction
Pressurization: Day 10	302	15.90	0.753	0.99566	2.24	2.84	NW/W
Depressurization: Day 7	225	12.1	0.746	0.99563	2.34	2.58	NW/W

[2]The term partial validity is used here to give emphasis on occurrence of acceptable outcomes which are independent of one another. In another word, an acceptable meteorological wind speed limit does not mean the requirement for wind speed limit at the height of building is satisfied or vice versa.

Table 4.5: Summary of Registered Deviations from Standard ISO 9972

			Deviations from Standard ISO 9972 - Test Parameters				
		Test #	Exponent n-value outside of acceptable limits ($0.5 \leq n \leq 1$).	Coefficient of Determination ($0.98 \leq r^2 \leq 1$)	Baseline pressure values is outside of acceptable limits	Interval between building pressures exceeds 10 Pa	Minimum pressure is not within +/- 3Pa of the greater of 10 Pa or (5 * zero-flow pressure $\Delta p01$)
Day 1	Pressurization	1-1A					
		2-1B					
		3-1B					
		4-1B					
		5-1B					
		6-1B					
		7-1B					
		8-1B					
		9-1B					
	Depressurization	1-1A					
		2-1A					
		3-1B					
		4-1B					
		5-1B					
		6-1B					
Day 2	Pressurization	1					
		2					
		3					
		4					
		5					
		6					
		7					
		8					
	Depressurization	1					
		2					
		3					
		4					
		5					
		6					
		7					
		8					
Day 3	Pressurization	1					
		2					
		3					
		4					
		5					
		6					
		7					
		8					
	Depressurization	1					
		2					
		3					
		4					
		5					
		6					
		7					
		8					

Continued on next page

Table 4.5 – *Continued from previous page*

			Deviations from Standard ISO 9972 - Test Parameters				
		Test #	Exponent n-value outside of acceptable limits ($0.5 \leq n \leq 1$).	Coefficient of Determination ($0.98 \leq r^2 \leq 1$)	Baseline pressure values is outside of acceptable limits	Interval between building pressures exceeds 10 Pa	Minimum pressure is not within +/- 3Pa of the greater of 10 Pa or (5 * zero-flow pressure .Δp01)
Day 4	Pressurization	1					
		2					
		3					
		4					
		5					
		6					
		7					
		8					
	Depressurization	1					
		2					
		3					
		4					
		5					
		6					
		7					
		8					
Day 5	Pressurization	1					
		2					
		3					
		4					
		5					
		6					
		7					
	Depressurization	1					
		2					
		3					
		4					
		5					
		6					
		7					
		8					
Day 6	Pressurization	1					
		2					
		3					
		4					
		5					
		6					
		7					
		8					
	Depressurization	1					
		2					
		3					
		4					
		5					
		6					
		7					
		8					

Continued on next page

Table 4.5 – *Continued from previous page*

			Deviations from Standard ISO 9972 - Test Parameters				
		Test #	Exponent n-value outside of acceptable limits ($0.5 \leq n \leq 1$).	Coefficient of Determination ($0.98 \leq r^2 \leq 1$)	Baseline pressure values is outside of acceptable limits	Interval between building pressures exceeds 10 Pa	Minimum pressure is not within +/- 3Pa of the greater of 10 Pa or (5 * zero-flow pressure .Δp01)
Day 7	Pressurization	1					
		2					
		3					
		4					
		5					
		6					
		7					
		8					
	Depressurization	1					
		2					
		3					
		4					
		5					
		6					
		7					
		8					
Day 8	Pressurization	1					
		2					
		3					
		4					
		5					
		6					
		7					
		8					
	Depressurization	1					
		2					
		3					
		4					
		5					
		6					
		7					
		8					
Day 9	Pressurization	1					
		2					
		3					
		4					
		5					
		6					
		7					
		8					
	Depressurization	1					
		2					
		3					
		4					
		5					
		6					
		7					
		8					

Continued on next page

Table 4.5 – *Continued from previous page*

		Deviations from Standard ISO 9972 - Test Parameters				
	Test #	Exponent n-value outside of acceptable limits ($0.5 \leq n \leq 1$).	Coefficient of Determination ($0.98 \leq r^2 \leq 1$)	Baseline pressure values is outside of acceptable limits	Interval between building pressures exceeds 10 Pa	Minimum pressure is not within +/- 3Pa of the greater of 10 Pa or (5 * zero-flow pressure .Δp01)
Day 10 Pressurization	1					
	2					
	3					
	4					
	5					
	6					
	7					
	8					
Depressurization	1					
	2					
	3					
	4					
	5					
	6					
	7					
	8					

4.2.2 Building Leakage Curve

The air leakage graphs presented in table 4.6 are comprised of several measurements of leakage air volumes at various pressure differences. The underlying parameters in equation 2.13 including air flow exponent (n) and air leakage coefficient (C_L), along with coefficient of determination (r^2) are investigated to reveal any valuable additional information that may correlate ALR with the measurement conditions.

Air Flow Exponent (n)

The air flow exponent (n) is an indication of the type of leaks that dominates the building. The results of both mode of measurements are valid in terms of the international standard ISO9972 as it is in the range 0.5 to 1. Generally, a trend with minimal deviation from an air flow exponent of 0.7 is displayed, which is often regarded as a good reference point (Tormod Aurlien, 2014). Practically, the air flow exponent is associated with large openings and holes for low air flow exponent, and with narrow cracks or leakage for high air flow exponent. The relatively stable air flow exponent around n = 0.7 may characterize the buildings envelope, and its variation due to the wind dynamics.

Air Leakage Coefficient (C_L)

The air flow coefficient C denotes the amount of air leaking into the building. It is obtained by correcting to the air flow coefficient, C_{env}, to standard conditions [20 °C and 1.013 x 10^5 Pa], using Equation 4.1 for depressurization and Equation 4.2 for pressurization:

$$C_L = C_{env}\left(\frac{\rho_e}{\rho_O}\right)^{1\text{-}n} \approx C_{env}\left(\frac{T_O}{T_e}\right)^{1\text{-}n} \tag{4.1}$$

where

- ρ_O is the air density at standard conditions, in kg/cubic meters
- T_O is the air absolute temperature at standard conditions, in K

$$C_L = C_{env}\left(\frac{\rho_{int}}{\rho_O}\right)^{1\text{-}n} \approx C_{env}\left(\frac{T_O}{T_{int}}\right)^{1\text{-}n} \tag{4.2}$$

Coefficient of Determination (r^2)

The coefficient of determination, r^2, provides some information about how well the regression curve fits the data samples. It assesses the linear relationship between the dependent variable (building target pressure [Pa]]) and the independent variable (building leakage [m^3/h]). The coefficient of determination is obtained separately for each measurement mode and shall not be less than 0.98 in order to produce the curve that best fits the data samples.

A closer look at the degree of variability in the building's leakage may be explained by the coefficient of determination as it is often considered a measures of "goodness of fit". Having stated that, caution must be taken when evaluating the meaning of this correlation. The coefficient of determination must not be presumed as a sole indicator for the quality of the data basis nor for the subsequent predictions.

The sampling process is subjected to varying wind situations which are taken insufficiently into account during the measurement process. Although an attempt is made by a pre- and post-test baseline measurements, any actual influence of wind during the sampling process remains unidentified. It is therefore believed that the coefficient of determination can be instrumental for identifying commonalities among the testes performed while conducting trend analysis under varying wind condition. With regard to the coefficient of determinations reported for this project, the requirement set by the standard is satisfied for 7 out of the 11 cases in the pressurization mode of measurements, and for 6 out of the 11 cases in the depressurization mode of measurements.

Leakage Curve Analysis

A preliminary analysis based on some observational markers may provide some insight which may also coincides with the underlying parameters discussed above. Four observational markers stand out; 1) large leaps along the regression curve, 2) lateral deviation from the regression curve, 3) differences in measured target pressure range, and 4) large differences among pressurization and depressurization measurement values.

Measurement devices and environmental conditions are considered the direct sources for the aforementioned observational markers(Tormod Aurlien, 2014). The observed deviations and instabilities can also be characterized as sources for a systematic or random error. While the source for systematic errors or bias can generally be corrected by equipment calibration, the nature[3] of the later error type does not allow for correction through calibration.

Large leaps and deviations from the regression curve along with achieved measurement of target pressure are dominant markers distinguishing the pressurization mode of measurements to the depressurization mode of measurements. The depressurization mode of measurements are observed to be be more close to each other and are found rarely in the vicinity of the lowest target pressure. Each mode of measurement exhibit building leakage rates that constitute values in the range of [300 - 400]$\frac{m^3}{h}$ for pressurization mode of measurement and [200-300]$\frac{m^3}{h}$ for depressurization mode of measurement at the highest target pressures.

On the opposite end of the leakage cure, leakage measurements are reported dominantly by the pressurization mode of measurement. For the depressurization mode of measurement, if the software fails to register the lowest target pressure line, the operator was prompted to change to the next lower flow ring. Thus,the absence of appropriate flow rings did not allow the execution of full range target pressure measurement. It is however an interesting observation that almost all pressurization mode of measurements were achieved by the flow rings provided. One should also bear in mind that the precise value of the target pressures were adjusted by a tolerance level ranging between 2Pa to 10Pa depending on the stability of the environmental conditions.

[3]Random error also known as precision, is a statistical error that is caused by chance and is not recurring.

Table 4.6: Overview of Building Leakage Test Result

Day 1

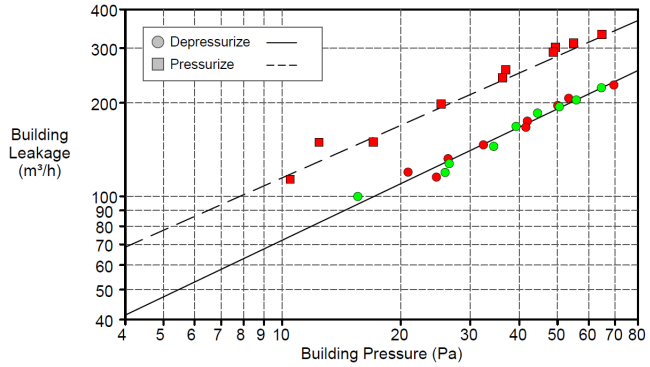

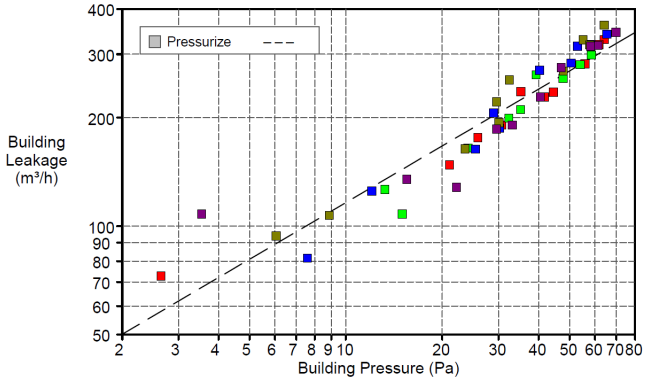

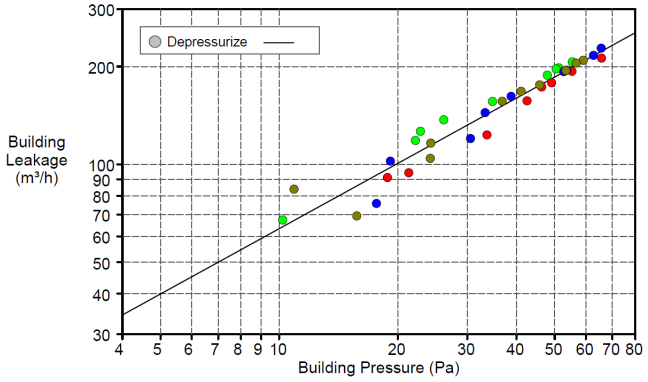

Day 2

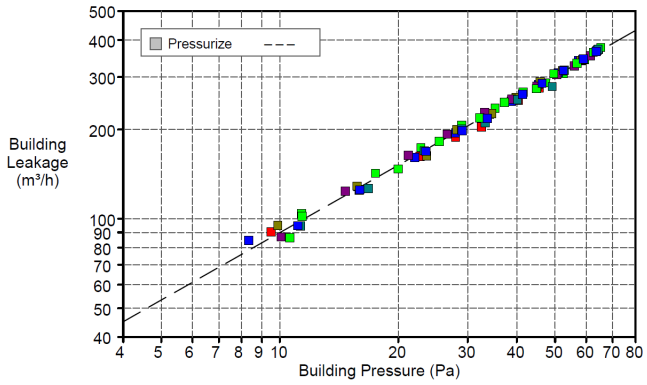

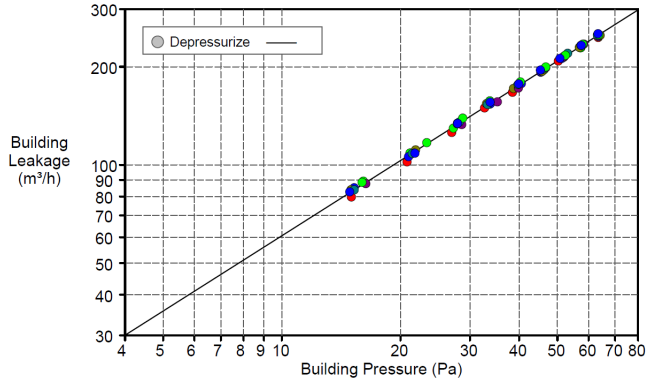

Day 3

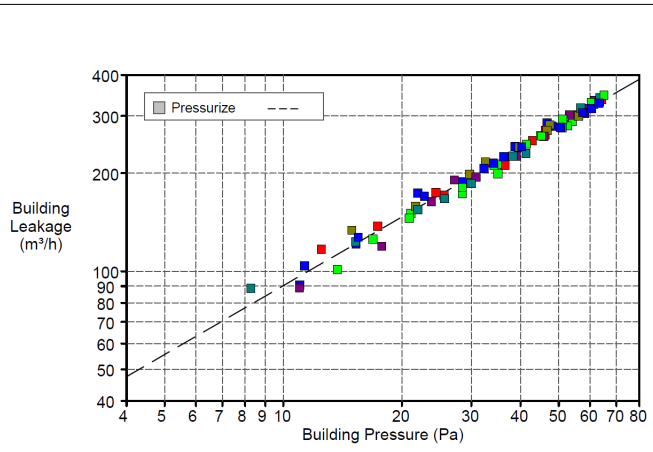

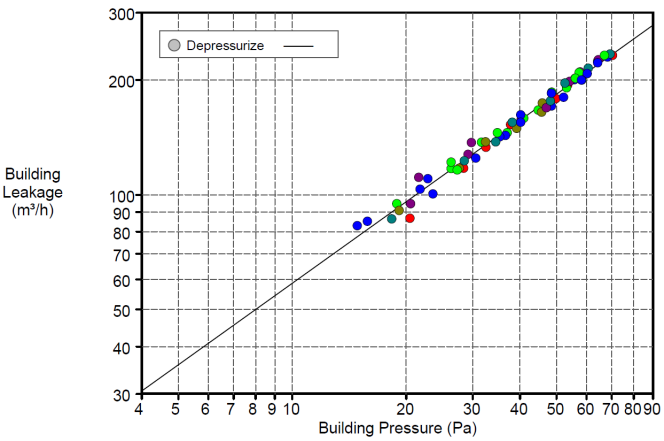

Table 4.6: (continued) Overview of Building Leakage Test Result

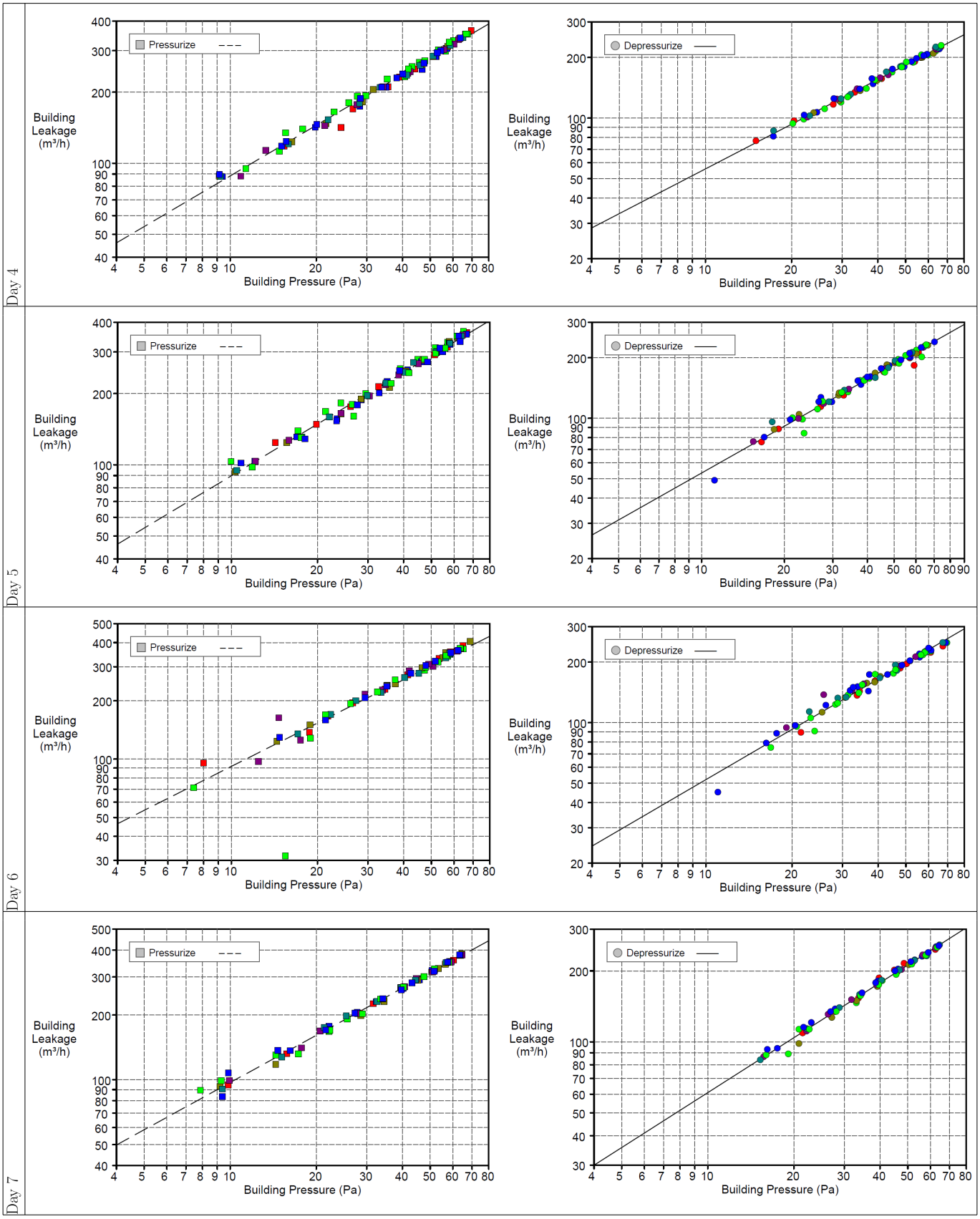

Table 4.6: (continued) Overview of Building Leakage Test Result

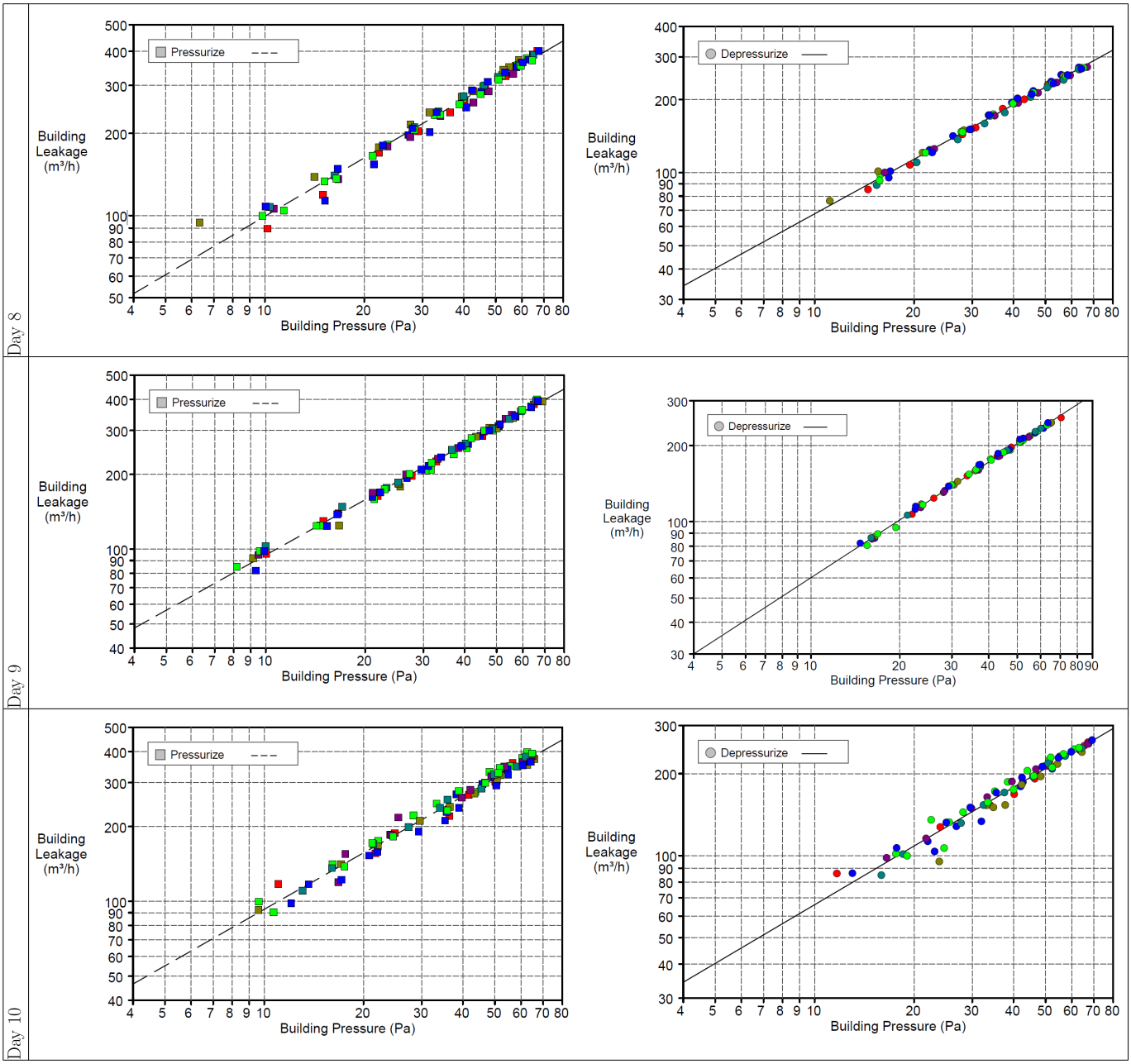

4.3 Analysis on Coefficient of Determination

Towards identifying the characteristic features of the R^2 value, scenarios that are deemed unsatisfactory (marked red) by the current standard are selected for further analysis. Firstly, a steady state wind analysis showing the correlation between the calculated mean wind speed and coefficient of determination is presented, followed by power spectrum analysis of the dynamic wind. Spectrum analysis is conducted to investigate further the role dynamic wind plays in the correlation mentioned. Each scenario offers a unique wind signal distribution for both wind speed and wind direction. Quantification of these parameters is an instrumental step towards establishing the role these parameters play on the degree of "goodness of fit". Probability density function (Pdf) provides such information by estimating the likely outcome of a discrete value, which in this study is the average value of either wind speed or wind direction.

4.3.1 Coefficient of Determination And Steady State Wind

A steady state approach indicates a high degree of correspondence between wind speed and the respective coefficient of determination. Deterioration in R^2 value can be observed while the average wind speed increment is roughly continuous. This is shown in Table 4.7 and Table 4.8 for the respective mode of measurements. The R^2 value in the tables mentioned seems to follow a trend that is inversely related to an increasing wind speed.

Table 4.7: Pressurization: Coefficient of Determination

		Wind Speed[$\frac{m}{s}$]			Wind Direction[θ_w]	
Test Day	R^2	Mean Speed	Probability density function Normal distribution	Probability density function Weibull distribution	Mean	Exposure Zone
Day 10	0.99566	2.24	0.4499	0.4289	296.4169	[WWN]
Day 8	0.99511	2.92	0.5256	0.4549	227.5659	[SW]
Day 6	0.99471	3.55	0.4235	0.3928	252.7078	[WWS]
Day 3	0.99151	4.33	0.2636	0.2506	353.7472	[NNW]
Day 4	0.98968	4.82	0.3427	0.3150	279.9403	[WWN]
Day 2	0.98515	4.03	0.3015	0.2867	162.7255	[SSE]
Day 7	0.98242	2.32	0.3276	0.3250	302.4302	[NW]
Day 9	0.97962	5.9	0.3129	0.2914	208.4336	[SSW]
Day 1A	0.93828	7.01	0.2301	0.2199	178.2021	[SSE]
Day 1B	0.89903	7.55	0.1919	0.1781	186.1113	[SSW]
Day 5	0.82193	7.15	0.1669	0.1486	254.3990	[WWS]

Although the descending trend of R^2 value complement our observation of the general steady state wind condition, the approach doesn't fully account for the occurrence of pattern breaks in the given order. For instance, the R^2 "goodness of fit" value for days such as Day 7 for the pressurization mode of measurement and Day 8 for the depressurization mode of measurement are poorly characterized by the steady state wind speed parameter despite the report of a relatively low wind speed.

Table 4.8: Depressurization: Coefficient of Determination

		Wind Speed[$\frac{m}{s}$]			Wind Direction[θ_w]	
Test Day	R^2	Mean Speed	Probability density function Normal distribution	Probability density function Weibull distribution	Mean	Exposure Zone
Day 10	0.99871	1.7218	0.5457	0.5222	277.4304	[WWN]
Day 8	0.99817	1.6338	0.4303	0.4428	247.0509	[WWS]
Day 7	0.99563	2.3416	0.3607	0.3501	282.1677	[WWN]
Day 3	0.99557	4.3091	0.2588	0.2434	11.6032	[NNE]
Day 6	0.99282	3.6732	0.3698	0.3460	278.5971	[WWN]
Day 2	0.98592	4.7778	0.3137	0.2907	176.9836	[SSE]
Day 4	0.97915	5.2948	0.2537	0.2312	280.3751	[WWN]
Day 1A	0.97508	7.5580	0.1927	0.1802	188.3780	[SSW]
Day 5	0.97466	7.5540	0.1855	0.1689	252.6940	[WWS]
Day 9	0.96174	6.0691	0.2567	0.2425	211.7289	[SW]
Day 1B	0.93826	7.0195	0.2068	0.1896	185.3449	[SSW]

Wind Roses

Another set of R^2 value characterization can be conducted by analysing the dominating wind direction with respect to the position of blower door device. Conveniently, the blower door is installed on the building's western facade, corresponding to an angular degree of $\theta_w = 270°$ west. Thus, serving as a reference angle for designating various exposure zones[4]. Consequently, the effect of wind exposure on the "goodness of fit" is investigated by comparing the calculated mean wind directions to the reference angle parameter.

The wind rose diagrams in Figure 4.1 illustrate pressurization measurements taken on Day 9, Day 1A, Day 1B and Day 5[5]. The wind speed in the direction of the prevailing wind at angle θ_w is also depicted. While Day 9 and Day 1B assume exposure zone [SSW], Day 1A and Day 5 are designated as [SSE] and [WWS] respectively.

Based on the angular difference between the exposure zone and the designated reference angle, $\theta_w = 270°$, the R^2 value may be expected to behave in the following descending order;[Day 1A - Day 1B - Day 9 - Day 5]. However, this appears to be not the case as estimate of the R^2 values are also affected by the wind strength. The combination of exposure zone and relatively strong wind condition seems to estimate a poor coefficient of determination on Day 5. Compared to Day 1A and Day 1B, the lower angular difference of Day 9 and the lower wind strength reported, seems to dominate estimation of its R^2 value.

[4]The term "exposure zone" may be understood as one of the angular sectors on a wind rose diagram from which wind is directed towards the Blower Door device. Example: S, SSW, SW, WWS, W, WWN, NW, NNW, N, NNE, NE, EEN, E, EES, SE, SSE

[5]The remaining wind roses are attached in appendix E

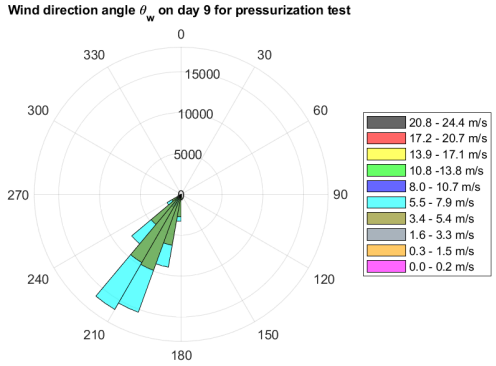

(a) Day 9: $\theta_w = 208.43°$ [SSW]

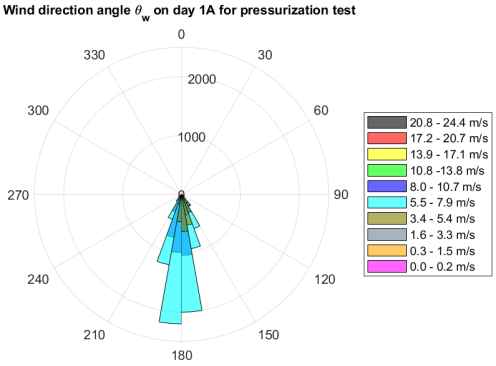

(b) Day 1A: $\theta_w = 178.20°$ [SSE]

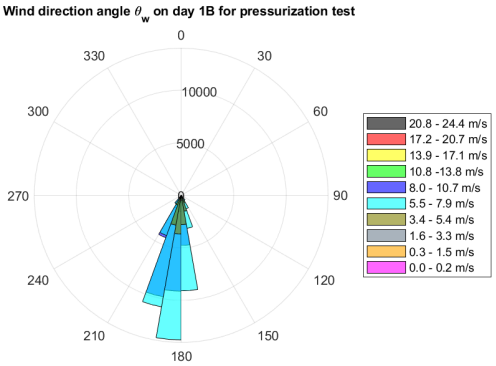

(c) Day 1B: $\theta_w = 186.11°$ [SSW]

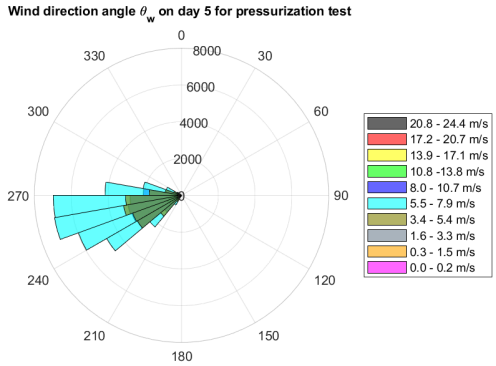

(d) Day 5: $\theta_w = 254.40°$ [WWS]

Figure 4.1: Pressurization measurement:Wind rose diagrams and prevailing wind direction for Day 9, Day 1A, Day 1B, and Day 6. ($\theta_w = 0°$ corresponds to North, $\theta_w = 90°$ corresponds to East, $\theta_w = 180°$ corresponds to South, $\theta_w = 270°$ corresponds to West)

The coefficient of determination estimated for Day 4, Day 1A, Day 5, Day 9 and Day 1B under depressurization measurement are presented in Table 4.8. The mode of measurement reports a total of five unsatisfactory R^2, which is one more than the pressurization mode of measurements. The test days have the following exposure zone; Day 4 [WWN], Day1A [SSW], Day 5 [WWS], Day 9 [SW], and Day 1B [SSW]. The discontinuity in trend development seems more evident in these mode of measurement.

The wind rose diagram 4.2a and angular difference calculation imply that the blower door measurement on Day 4 is more susceptible for direct exposure to wind, followed by Day 5 - Day 9 - Day 1A - Day 1B in that descending order. While the wind strength reported on Day 5 and Day 1A are similar in value, the angular difference to the reference angle, $\theta_w = 270°$, is calculated to be less for Day 5 than Day 1A. Such combination is expected to inform a poor "goodness to fit" value for Day 5. However, the reported R^2 values for Day 5 and Day 1A indicates a better "goodness of fit" than Day 9 and Day 1B, where the later pair have reported lower wind strength relatively large angular distance to the reference angle. Assessment of the R^2 values based on the combined effect of exposure zone and wind strength fails to fully account for the reported coefficient of determinations.

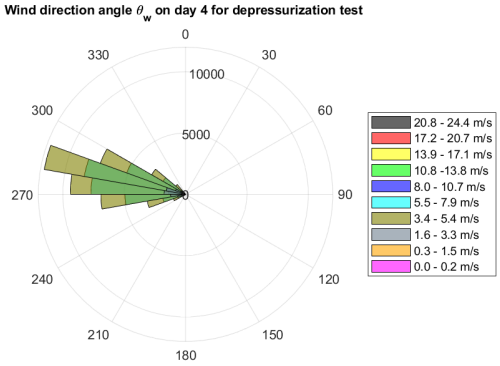

(a) Day 4: $\theta_w = 280.37°$ [WWN]

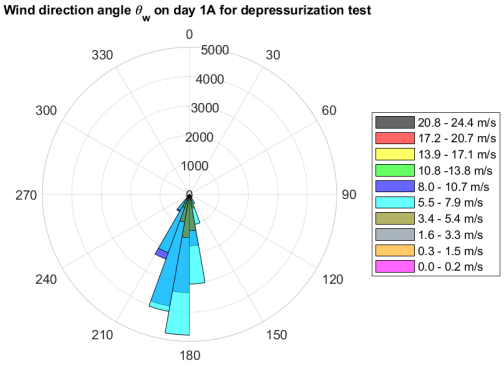

(b) Day 1A: $\theta_w = 188.38°$ [SSW]

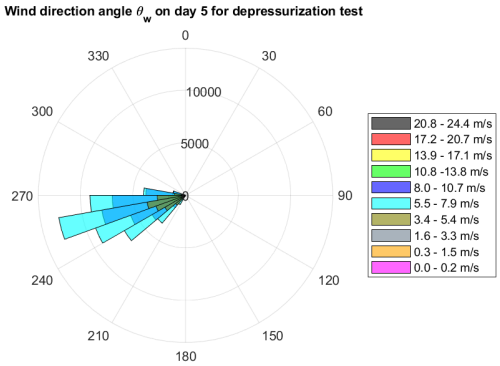

(c) Day 5: $\theta_w = 252.69°$ [WWS]

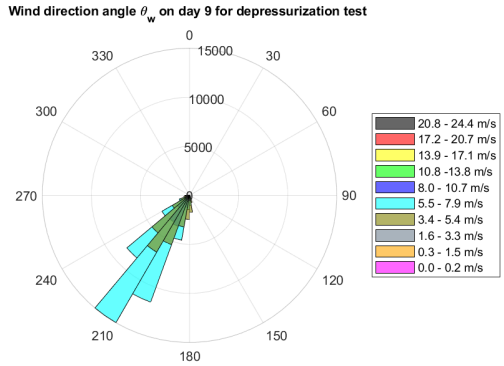

(d) Day 9: $\theta_w = 211.73°$ [SW]

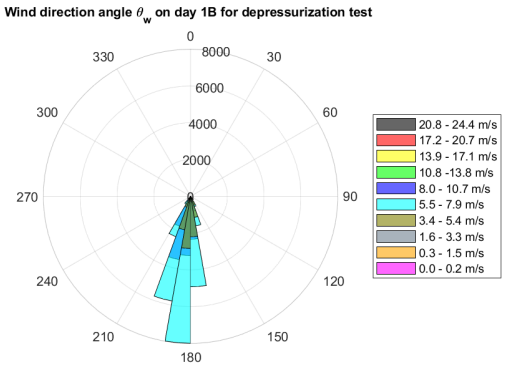

(e) Day 1B: $\theta_w = 185.34°$ [SSW]

Figure 4.2: Depressurization measurement: Wind rose diagrams and prevailing wind direction for Day 4, Day 1A, Day 5, Day 9, Day1B. ($\theta_w = 0°$ corresponds to North, $\theta_w = 90°$ corresponds to East, $\theta_w = 180°$ corresponds to South, $\theta_w = 270°$ corresponds to West)

4.3.2 Coefficient of Determination And Spectral Analysis

A wind power spectrum $S_{xy}(f)$ along with time series for wind signal of the pressurization and depressurization mode of measurements are partially presented in Figure 4.3 and Figure 4.4 respectively. The remaining wind power spectrum are attached in appendix D. This approach provides an opportunity to examine the wind fluctuation frequency and assess the impact of dynamic wind on the estimation of the coefficient of determination.

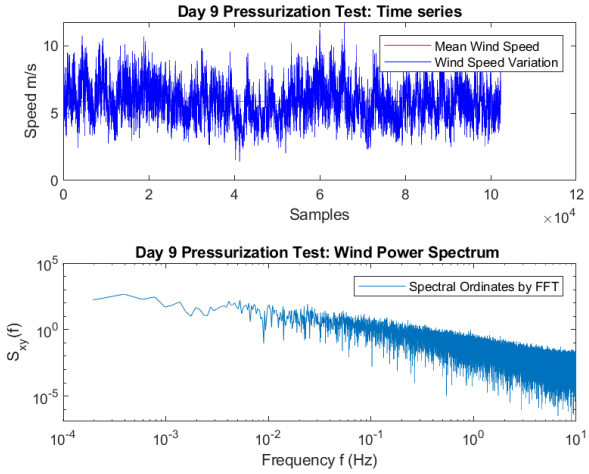

(a) Day 9

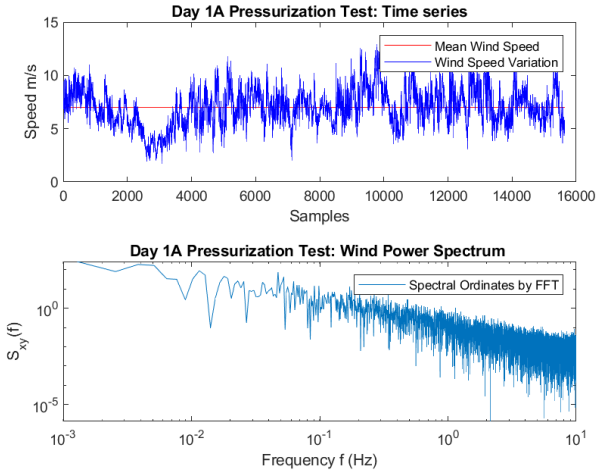

(b) Day 1A

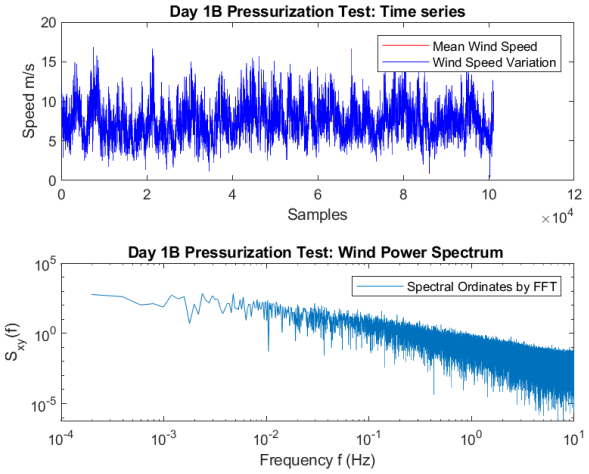

(c) Day 1B

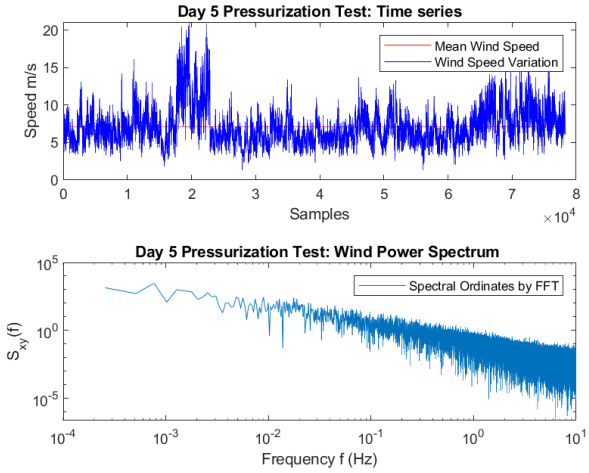

(d) Day 5

Figure 4.3: Pressurization measurement: Wind power spectra $S_{xy}(f)$

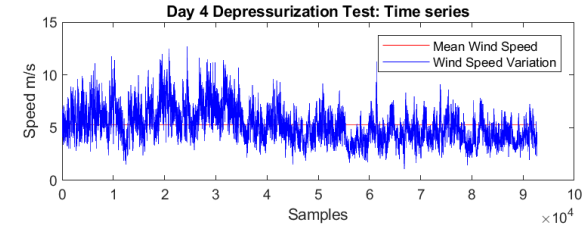

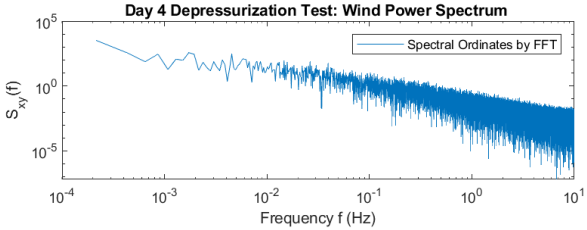

(a) Day 4

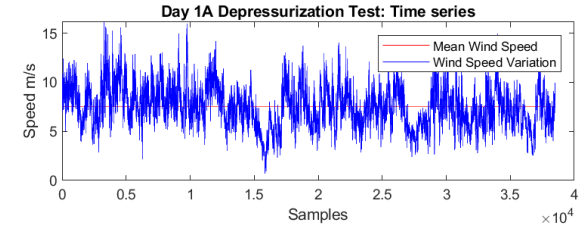

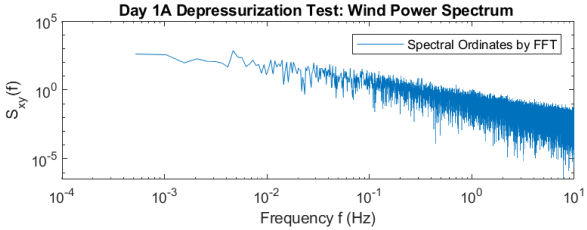

(b) Day 1A

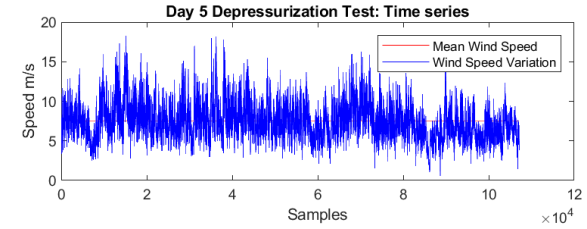

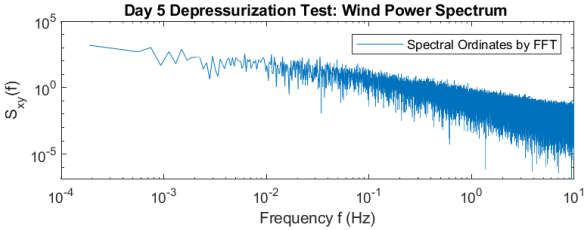

(c) Day 5

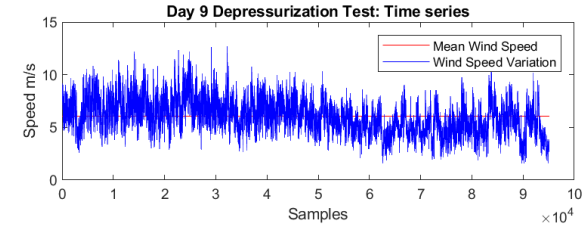

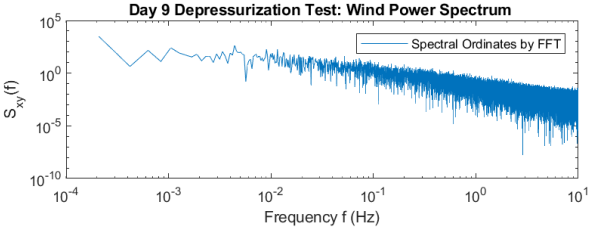

(d) Day 9

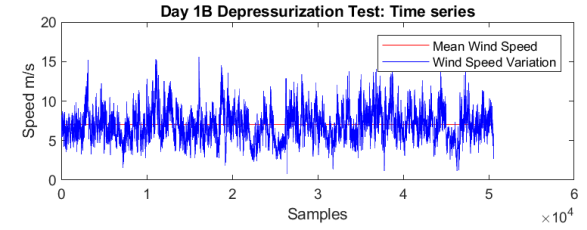

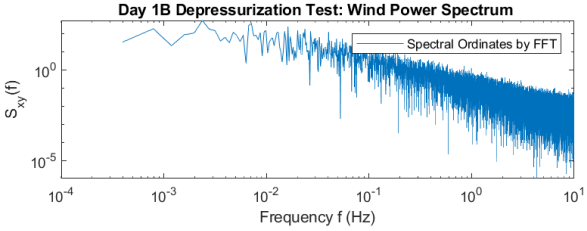

(e) Day 1B

Figure 4.4: Depressurization measurement: Wind power spectra $S_{xy}(f)$

In order to perform spectral analysis and extract the information contained in the signal spectrum, further smoothing of the curves is required. Application of such procedure has produced Figure 4.5 and 4.6 for pressurization and depressurization mode of measurements.

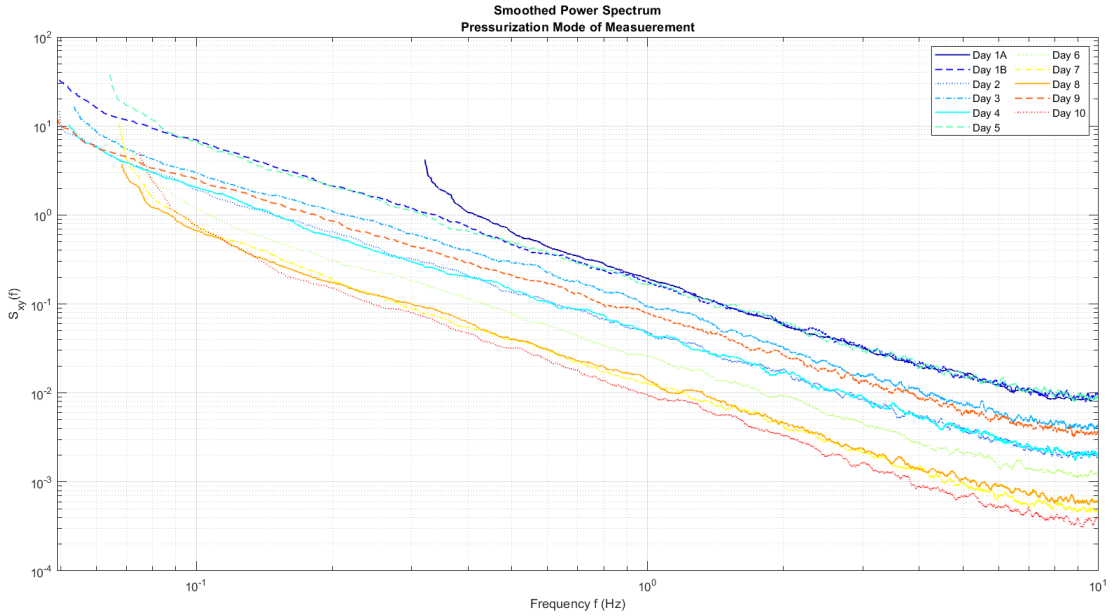

Figure 4.5: Pressurization Test: Smoothed Power Spectrum

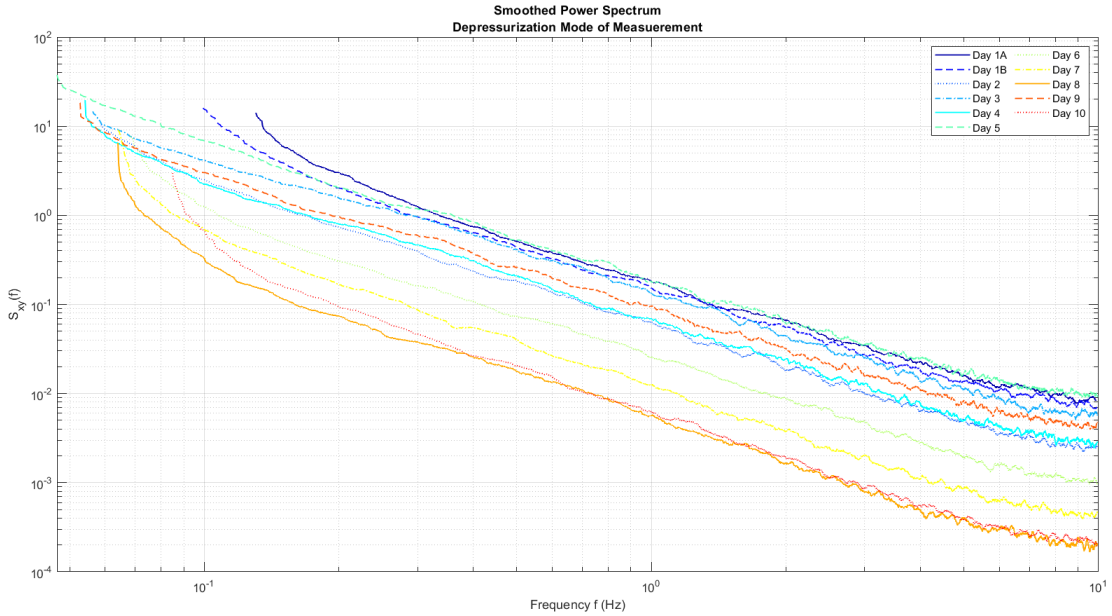

Figure 4.6: Depressurization Test: Smoothed Power Spectrum

So far, R^2 values that were deemed unsatisfactory were evaluated based on a steady state wind condition and wind direction. Such analysis on the unsatisfactory R^2 values of pressurization mode of measurements was able to provide the rational for the reported R^2 results. On the contrary, the R^2 values for the depressurization

mode of measurements were not explained by the same token.

The wind power spectrum $S_{xy}(f)$ for pressurization mode of measurements in Figure 4.3 affirms the observation and analysis made by steady state wind condition and wind direction. The energy density distribution for Day 1B and Day 5 run close to each other in alternating pattern across the whole frequency domain. Day 1A is also noticed to as part of this alternating pattern before it clearly breaks off and attend a higher energy density level for frequency interval f $\approx<$ 1.2 Hz. The energy density for Day 9 follows its own course across the frequency domain with a lower energy density distribution.

The spectral analysis for the depressurization mode of measurement is presented in Figure 4.4. In the frequency domain of $0.3Hz < f < 10Hz$, the energy density of Day 5 dominates the spectrum, while the energy density of Day 1A is observed at times to overtake. At $f \approx> 0.3Hz$ do spectrum of Day 1A succeeds and becomes dominant. The spectrum of Day 1B appears to do the same and overtakes the spectrum of Day 5 at $f \approx> 0.16Hz$. The power spectrum for Day 9 follows its own course across the frequency domain with a lower energy density distribution.

In order to address the reported R^2 values in accordance with spectral analysis, energy densities at low frequency must be given a considerable attention. In spite of the wind strength and assumed exposure zone, the coefficient of determination obtained by Day 1B can in part be accounted by the energy density it exhibits at low frequency domain.

4.3.3 Coefficient of Determination And Wind speed Probability Density Function

The probability density function illustrates the likelihood of finding the prevailing wind speed during the measurement. Table 4.9 and Table 4.10 tend to indicate a general trend of decreasing probability estimation as the R^2 value decreases. However, the trend is inconsistent in the same manner as it was discussed in earlier sections.

Table 4.9: Pressurization Mode of Measurement: Wind Speed Probability Distribution Function

		Wind Speed[$\frac{m}{s}$]			Wind Direction[θ_w]	
Test Day	R^2	Mean Speed	Probability density function Normal distribution	Probability density function Weibull distribution	Mean	Exposure Zone
Day 10	0.99566	2.24	0.4499	0.4289	296.4169	[WWN]
Day 8	0.99511	2.92	0.5256	0.4549	227.5659	[SW]
Day 6	0.99471	3.55	0.4235	0.3928	252.7078	[WWS]
Day 3	0.99151	4.33	0.2636	0.2506	353.7472	[NNW]
Day 4	0.98968	4.82	0.3427	0.3150	279.9403	[WWN]
Day 2	0.98515	4.03	0.3015	0.2867	162.7255	[SSE]
Day 7	0.98242	2.32	0.3276	0.3250	302.4302	[NW]
Day 9	0.97962	5.9	0.3129	0.2914	208.4336	[SSW]
Day 1A	0.93828	7.01	0.2301	0.2199	178.2021	[SSE]
Day 1B	0.89903	7.55	0.1919	0.1781	186.1113	[SSW]
Day 5	0.82193	7.15	0.1669	0.1486	254.3990	[WWS]

Table 4.10: Depressurization Mode of Measurement: Wind Speed Probability Distribution Function

		Wind Speed[$\frac{m}{s}$]			Wind Direction[θ_w]	
Test Day	R^2	Mean Speed	Probability density function Normal distribution	Probability density function Weibull distribution	Mean	Exposure Zone
Day 10	0.99871	1.7218	0.5457	0.5222	277.4304	[WWN]
Day 8	0.99817	1.6338	0.4303	0.4428	247.0509	[WWS]
Day 7	0.99563	2.3416	0.3607	0.3501	282.1677	[WWN]
Day 3	0.99557	4.3091	0.2588	0.2434	11.6032	[NNE]
Day 6	0.99282	3.6732	0.3698	0.3460	278.5971	[WWN]
Day 2	0.98592	4.7778	0.3137	0.2907	176.9836	[SSE]
Day 9	0.96174	6.0691	0.2567	0.2425	211.7289	[SW]
Day 4	0.97915	5.2948	0.2537	0.2312	280.3751	[WWN]
Day 1B	0.93826	7.0195	0.2068	0.1896	185.3449	[SSW]
Day 1A	0.97508	7.5580	0.1927	0.1802	188.3780	[SSW]
Day 5	0.97466	7.5540	0.1855	0.1689	252.6940	[WWS]

The estimates for the peak wind speed by the probability density functions are generally higher for Normal distribution than Weibull distribution function. The peak of the probability density functions denote the most frequent velocity for each scenario, and are presented in Table 4.11 and Table 4.12 for the respective mode of measurements. The confidence interval for the scale factor and shape factor is presented in appendix G.

The parameter denoting the wind speed carrying maximum energy $V_{\text{xy}\,MaxE}$ appears to provide a better indication of the correlation R^2 values have with wind strength variation. Day 2 and Day 7 for the pressurization mode of measurements, and Day 6 for the depressurization mode of measurement differ from the pattern observed.

Table 4.11: Pressurization Mode of Measurement: Weibull Pdf-Parameters and Significant Wind Speeds

Test Day	R^2	Mean speed	Weibull Pdf	Peak wind speed	Scale factors c	Shape parameter k	Most probable wind speed $V_{\text{xy}\,pdf}$	Wind speed carrying maximum energy $V_{\text{xy}\,MaxE}$
Day 10	0.99566	2.2396	0.4289	2.1193	2.5160	2.7125	2.1236	3.0843
Day 8	0.99511	2.9239	0.4549	2.9667	3.2155	3.8299	2.9712	3.5883
Day 6	0.99471	3.5511	0.3928	3.6450	3.9098	4.0373	3.6437	4.3196
Day 3	0.99151	4.3331	0.2506	4.2827	4.8466	3.1144	4.2799	5.6834
Day 4	0.98968	4.8257	0.3150	4.9837	5.2816	4.3978	4.9806	5.7515
Day 2	0.98515	4.0267	0.2867	4.0270	4.4876	3.3244	4.0297	5.1707
Day 7	0.98242	2.3210	0.3250	1.8180	2.6128	1.9689	1.8226	3.7302
Day 9	0.97962	5.8967	0.2914	6.1318	6.4108	4.9681	6.1273	6.8626
Day 1A	0.93828	7.0156	0.2199	7.2633	7.6826	4.4699	7.2595	8.3452
Day 1B	0.89903	7.5529	0.1781	7.7170	8.3335	3.8910	7.7210	9.2708
Day 5	0.82193	7.1505	0.1486	6.9890	7.9801	3.0313	6.9928	9.4319

Table 4.12: Depressurization Mode of Measurement: Weibull Pdf- Parameters and Significant Wind Speeds

Test Day	R^2	Mean speed	Weibull Pdf	Peak wind speed	Scale factors c	Shape parameter k	Most probable wind speed $V_{\text{xy}\,pdf}$	Wind speed carrying maximum energy $V_{\text{xy}\,MaxE}$
Day 10	0.99871	1.7218	0.5222	1.5787	1.9363	2.5042	1.5797	2.4478
Day 8	0.99817	1.6338	0.4428	1.2025	1.8421	1.8435	1.2054	2.7442
Day 7	0.99563	2.3416	0.3501	2.0132	2.6381	2.2248	2.0173	3.5195
Day 3	0.99557	4.3091	0.2434	4.2149	4.8261	2.9971	4.2147	5.7236
Day 6	0.99282	3.6732	0.3460	3.7371	4.0697	3.6744	3.7327	4.5807
Day 2	0.98592	4.7778	0.2907	4.9030	5.2601	4.0179	4.8984	5.8164
Day 9	0.96174	6.0691	0.2425	6.2569	6.6654	4.2639	6.2605	7.2946
Day 4	0.97915	5.2948	0.2312	5.3481	5.8723	3.5296	5.3435	6.6688
Day 1B	0.93826	7.0195	0.1896	7.1635	7.7440	3.8461	7.1609	8.6347
Day 1A	0.97508	7.5580	0.1802	7.7375	8.3335	3.9409	7.7370	9.2482
Day 5	0.97466	7.5540	0.1689	7.6622	8.3522	3.6818	7.6633	9.3967

Calculation of the most probable wind speed corresponds to the peak probability density function. The pdf for all measurements is depicted in Figure 4.7.

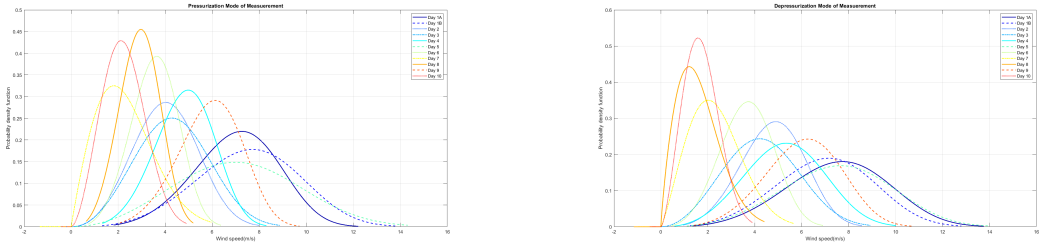

(a) Wind speed distribution for pressurization mode of measurement.

(b) Wind speed distribution for depressurization mode of measurement.

Figure 4.7: Overview of wind speed Weibull probability density distribution.

The Normal and Weibull distribution function are graphically compared in Figure 4.8 and 4.9. The peak of the density function in Weibull distribution are skewed towards the higher values of mean wind speed. A very clear representation becomes evident on Day 7 for the respective mode of meaurement.

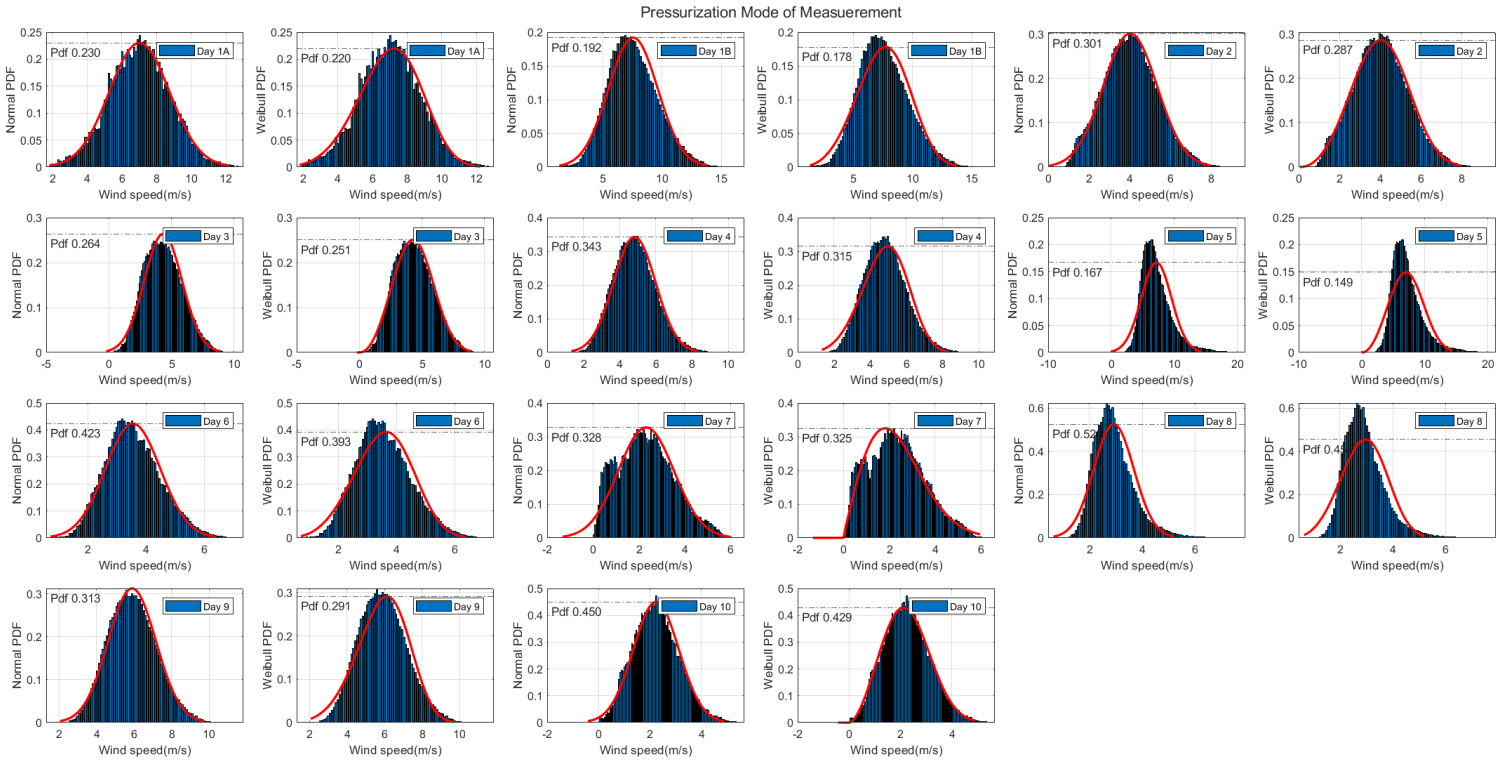

Figure 4.8: Comparing the normal and weibull pdf for wind speed of pressurization mode of measurement.

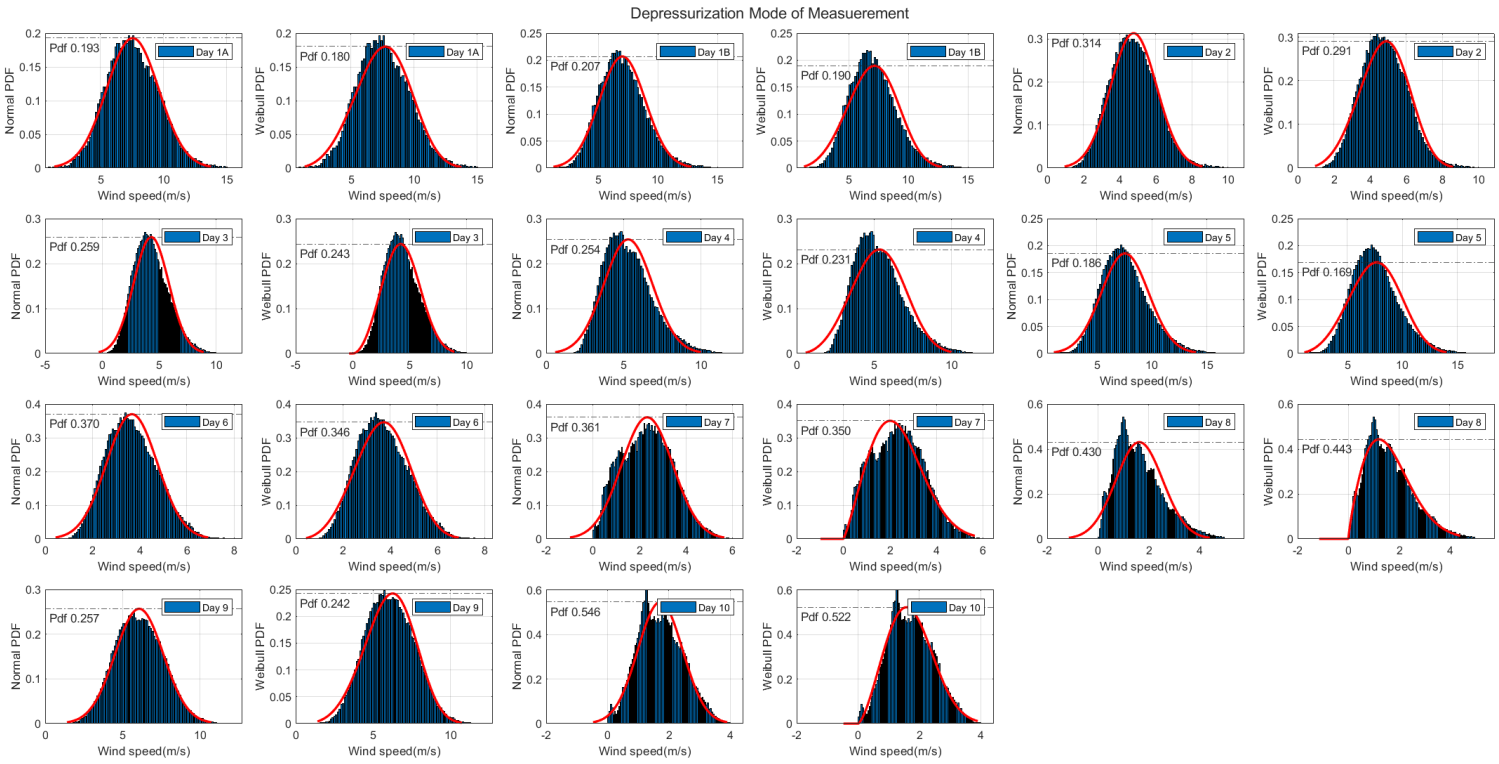

Figure 4.9: Comparing the normal and weibull pdf for wind speed of depressurization mode of measurement.

Chapter 5

Conclusion

The purpose of this this thesis is to conduct an experimental study and analyse the impact and consequences of dynamic wind on the fan pressurization method. The ISO9972 standard provides the guidelines that should be followed when performing airtightness measurements and how uncertainties should be handled. In spite of those efforts, the effect of dynamic wind during the measurement itself is not fully considered. Towards quantifying these uncertainties, an analysis on declared airtightness is conducted. The coefficient of determination, also known as " goodness of fit", is selected to investigate the impact dynamic wind exerts on the fan pressurization method.

The following concluding remarks are made based on the result and analysis presented.

- The impact assessment of dynamic wind condition can be considered an amalgamation of the following factors:
  - The strength of wind signal appears to reside not only in its speed, but also direction, more specifically, the degree of its spread relative to the blower door equipment. In another word, angular exposure of the blower door to the direction of the prevailing wind speed.
  - Spectral energy distribution at low frequencies or the gustiness the wind
  - The wind speed carrying the maximum energy.
- The wind speed that carries the maximum amount of wind energy can be identified based on the best fitting probability distribution function. It can pinpoint the maximum amount of wind energy associated with different measurements procedures under various wind condition.
- Identifying the impact of dynamic wind on the fan pressurization method demands an accurate description of the actual data. To wards that goal, the best fitting distribution function must be systematically selected. A statistical analysis can be applied to evaluate the performance of any chosen distribution function.
- A wind rose diagram depicts an uneven distribution of wind in each direction. Such variation necessitates considering its relevance during fan pressurization measurement besides wind velocity. A study of distribution models that combine these two parameters is recommended.
- The R^2 values obtained in this study, and the quality of their "goodness to fit" implicates the approach utilized by ISO9972 as a rather conservative design.

Recommendations for future work

- A comparative study of various distribution function is with regard to selecting the best fitting distribution function.
- The influence of vertical axis wind velocity is ignored in this thesis. Identifying the impact it poses on the coefficient of determination and on the air leakage rate, may provide close a knowledge gap and enhances the understanding of the air leakage rate.
- The role played by the wind speed, carrying the maximum energy, can be an area of study that may uncover the uncertainties associated with fan pressurization method outside of the scope of ISO9972. in estimating the "Fan pressurization design limit", or in quantifying the measurement uncertainty
- A multivariate analysis is recommended to quantify any significant correlations between the wind signal data analysed.

References

Akdağ, S. A., & Dinler, A. (2009). A new method to estimate weibull parameters for wind energy applications. *Energy conversion and management*, *50*(7), 1761–1766.

Akins, R. E. (1976). Wind pressures on buildings. *CER; 76/77-15*.

American Meteorological Society. (2019, sep). *aerodynamic roughness length.* Retrieved on 10.03.2020, from `http://glossary.ametsoc.org/wiki/Aerodynamic_roughness_length`

ASTM International. (2019, Jan). *Standard test method for determining air leakage rate by fan pressurization* (Standard No. ISO 9972:2015)). Online. West Conshohocken, PA. Retrieved from `http://www.astm.org/cgi-bin/resolver.cgi?E779-19`

Berge, A. (2011). Analysis of methods to calculate air infiltration for use in energy calculations.

Bracke, W., Laverge, J., Bossche, N. V. D., & Janssens, A. (2016). Durability and measurement uncertainty of airtightness in extremely airtight dwellings. *International Journal of Ventilation*, *14*(4), 383–394.

Brit Roald, R. D. S. o. I. L. S. (2017, aug). *Nullutslippsbygninger (zeb). retningslinjer og beregningsmetoder* (Series No. 473.020). Forskningsveien 1, 0373 Oslo: SINTEF Byggforsk. (ISSN 2387-6328)

Carrié, F., Jobert, R., & Leprince, V. (2012). Methods and techniques for airtight buildings. *Air Infiltration and Ventilation Centre, Coventry, UK*.

Carrie, F., & Wouters, P. (2012). Building airtightness: a critical review of testing, reporting and quality schemes in 10 countries. *TightVent Europe. CIBSE (2000). Testing buildings for air leakage, CIBSE Technical Memorandum*, *23*.

CEN, E. C. f. S. (2015, dec). *Thermal performance of buildings - determination of air permeability of buildings - fan pressurization method (iso 9972:2015)* (Standard No. ISO 9972:2015)). Online. Postboks 252, 1326 Lysaker. Retrieved from `https://www-standard-no.ezproxy.hioa.no/no/Nettbutikk/produktkatalogen/Produktpresentasjon/?ProductID=790369` (his standard is intended for the measurement of the air permeability of buildings or parts of buildings in the field. It specifies the use of mechanical pressurization or depressurization of a building or part of a building. It describes the measurement of the resulting air flow rates over a range of indoor-outdoor static pressure differences. This standard is intended for the measurement of the air leakage of building envelopes of single-zone buildings.)

Chadee, J. C., & Sharma, C. (2001). Wind speed distributions: A new catalogue of defined models. *Wind Engineering*, *25*(6), 319-337. Retrieved from `https://doi.org/10.1260/030952401760217139` doi: 10.1260/030952401760217139

Chan, W. R., Joh, J., & Sherman, M. H. (2013). Analysis of air leakage measurements of us houses. *Energy and Buildings*, *66*, 616–625.

Chiu, Y., & Etheridge, D. (2002). Calculations and notes on the quadratic and power law equations for modelling infiltration. *International journal of ventilation*, *1*(1), 65–77.

Delmotte, C. (2017). Airtightness of buildings-considerations regarding the zero-flow pressure and the weighted line of organic correlation. In *38th aivc conference" ventilating healthy low-energy buildings.*

Etheridge, D. (1977). Crack flow equations and scale effect. *building and environment*, *12*(3), 181–189.

Etheridge, D. (1998). A note on crack flow equations for ventilation modelling. *Building and Environment*, *33*(5), 325–328.

European Commission. (2011, dec). Energy roadmap 2050. *SEC (2011)*, *1565*.

European Parliament. (2018, jun). *European directive 2018/844 amending directive 2010/31/eu on the energy performance of buildings and directive 2012/27/eu on energy efficiency.* Official Journal of the European Union. Vol. 156.

Favi, C., Di Giuseppe, E., D'Orazio, M., Rossi, M., & Germani, M. (2018). Building retrofit measures and design: a probabilistic approach for lca. *Sustainability*, *10*(10), 3655.

Gill Instruments. (2010, feb). Windmaster (part 1590-pk-020) & windmaster pro(part 1561-pk-020) ultrasonic anemometer user manual (Doc No. 1561-PS-0001 Issue 06 ed.) [Computer software manual]. Saltmarsh Park,67 Gosport Street, Lymington,Hampshire. SO41 9EG UK.

Ginger, J., & Letchford, C. (1999). Net pressures on a low-rise full-scale building. *Journal of Wind Engineering and Industrial Aerodynamics*, *83*(1-3), 239–250.

Google Maps. (2020, mar). *Ås.* Retrieved on 10.03.2020, from `https://goo.gl/maps/puQmsyVBpvzE9Hy48`

Gullbrekken, L., Uvsløkk, S., Kvande, T., Pettersson, K., & Time, B. (2018). Wind pressure coefficients for roof ventilation purposes. *Journal of Wind Engineering and Industrial Aerodynamics*, *175*, 144–152.

Haghighat, F., Brohus, H., & Rao, J. (2000). Modelling air infiltration due to wind fluctuations—a review. *Building and Environment*, *35*(5), 377–385.

Hussain, M., & Lee, B. (1980). A wind tunnel study of the mean pressure forces acting on large groups of low-rise buildings. *Journal of Wind Engineering and Industrial Aerodynamics*, *6*(3-4), 207–225.

IEA, I. E. A. (2017). *Energy policies of iea countries: Norway 2017 review.* Retrieved on 23.01.2020, from `https://www.iea.org/reports/energy-policies-of-iea-countries-norway-2017-review`

IEA, I. E. A. (2020, jan). *World energy balances and statistics.* Retrieved on 23.01.2020, from `https://www.iea.org/subscribe-to-data-services/world-energy-balances-and-statistics`

Jesús, F.-M., Cristina, P., Víctor, E., Jesica, F.-A., Assiego de Larriva, R., Montesdeoca, M., ... Meiss, A. (2019, 02). Energy impact of the air infiltration in residential buildings in the mediterranean area of spain and the canary islands. *Energy and Buildings*, *188*. doi: 10.1016/j.enbuild.2019.02.023

Jo, J.-H., Lim, J.-H., Song, S.-Y., Yeo, M.-S., & Kim, K.-W. (2007). Characteristics of pressure distribution and solution to the problems caused by stack effect in high-rise residential buildings. *Building and Environment*, *42*(1), 263–277.

Jokisalo, J., Kurnitski, J., Korpi, M., Kalamees, T., & Vinha, J. (2009, 02). Building leakage, infiltration, and energy performance analyses for finnish detached houses. *Building and Environment*, *44*, 377-387. doi: 10.1016/j.buildenv.2008.03.014

Khoukhi, M., & Al-Maqbali, A. (2011). Stack pressure and airflow movement in high and medium rise buildings. *Energy Procedia*, *6*, 422–431.

Kraniotis, D. (2014). *Dynamic characteristics of wind-driven air infiltration in buildings - the impact of wind gusts under unsteady wind conditions* (Doctoral dissertation). doi: 10.13140/RG.2.1.3607.9444

Kronvall, J. (1980). *Air flows in building components.* Division of Building Technology, Lund Institute of Technology Lund.

Leprince, V., & Carrié, F. (2018, 06). Uncertainties due to steady wind in building pressurisation tests. , 13-14.

Leprince, V., Moujalled, B., & Litvak, A. (2017). Durability of building airtightness, review and analysis of existing studies. In *Proceedings of the 38th aivc conference ventilating healthy low-energy buildings, nottingham, uk* (pp. 13–14).

Liddament, M. W. (1986). *Air infiltration calculation techniques: An applications guide.* Air infiltration and ventilation centre Berkshire, UK.

Lstiburek, J., Pressnail, K., & Timusk, J. (2002). Air pressure and building envelopes. *Journal of Thermal Envelope and Building Science*, *26*(1), 53–91.

Luis, A.-L. J. (2015). An approximation to the probability normal distribution and its inverse. *Ingeniería, Investigación y Tecnología*, *16*(4), 605–611.

MATLAB. (2020a, jun). *Normal distribution.* Natick, Massachusetts: The MathWorks Inc. Retrieved on 09.06.2020, from `https://www.mathworks.com/help/stats/normal-distribution.html`

MATLAB. (2020b, jun). *Weibull distribution.* Natick, Massachusetts: The MathWorks Inc. Retrieved on 09.06.2020, from `https://www.mathworks.com/help/stats/weibull-distribution.html`

Mazzeo, D., Oliveti, G., & Labonia, E. (2018). Estimation of wind speed probability density function using a mixture of two truncated normal distributions. *Renewable Energy*, *115*, 1260–1280.

McWilliams, B., Newmann, M., & Sprevak, D. (1979). The probability distribution of wind velocity and direction. *Wind Engineering*, *3*(4), 269–273. Retrieved from `http://www.jstor.org/stable/43749150`

McWilliams, J. (2002). Review of air flow measurement techniques.

Morgan, V. T. (1995). Statistical distributions of wind parameters at sydney, australia. *Renewable Energy*, *6*(1), 39–47.

Muehleisen, R. T., & Patrizi, S. (2013). A new parametric equation for the wind pressure coefficient for low-rise buildings. *Energy and Buildings*, *57*, 245–249.

Newland, D. E. (2012). *An introduction to random vibrations, spectral & wavelet analysis.* Courier Corporation.

O'Haver, P. T. (2019, dec). *A pragmatic introduction to signal processing.* Retrieved on 04.06.2020, from `https://terpconnect.umd.edu/~toh/spectrum/SmoothingComparison.html`

Ohkuma, T., Marukawa, H., Niihori, Y., & Kato, N. (1991). Full-scale measurement of wind pressures and response accelerations of a high-rise building. *Journal of Wind Engineering and Industrial Aerodynamics*, *38*(2-3), 185–196.

Orme, M., Liddament, M. W., & Wilson, A. (1998). *Numerical data for air infiltration and natural ventilation calculations.* Air Infiltration and Ventilation Centre Bracknell.

Oyedepo, S. O., Adaramola, M. S., & Paul, S. S. (2012). Analysis of wind speed data and wind energy potential in three selected locations in south-east nigeria. *International Journal of Energy and Environmental Engineering*, *3*(1), 7.

Poza-Casado, I., Meiss, A., Padilla-Marcos, M., & Feijó-Muñoz, J. (2019, 10). Airtightness and energy impact of air infiltration in residential buildings in spain..

Prignon, M., Dawans, A., Altomonte, S., & Van Moeseke, G. (2019, 02). A method to quantify uncertainties in airtightness measurements: Zero-flow and envelope pressure. *Energy and Buildings*. doi: 10.1016/j.enbuild.2019.02.006

Prignon, M., Dawans, A., & Van Moeseke, G. (2018, 09). Uncertainties in airtightness measurements: regression methods and pressure sequences..

Redaksjonen. (2019, nov). *Vind og lufttrykk.* Retrieved on 19.05.2020, from `https://www.nmbu.no/fakultet/realtek/laboratorier/bioklim/maleinstrumenter/vind`

Shaw, C. Y. (1981). Correlation between air infiltration and air tightness for houses in a developed residential area. *ASHRAE Trans.;(United States)*, *87*(CONF-810657-).

Sherman, M., & Chan, R. (2004, 01). Building airtightness: Research and practice: Lawrence berkeley national laboratory report no. lbnl-53356. *Lawrence Berkeley National Laboratory*.

Stoica, P., Moses, R. L., et al. (2005). Spectral analysis of signals.

Tamblyn, R. (1991). Coping with air pressure problems in tall buildings. *Ashrae Transactions*, *97*(1), 824–827.

The Energy Conservatory. (2007a). Minneapolis blower door™ operation manual for model 3 and model 4 systems [Computer software manual].

The Energy Conservatory. (2007b). Tectite express (ver. 3.6 for windows) (building airtightness test analysis program), software user's guide [Computer software manual].

Tormod Aurlien, M. S., Sverre Holøs (Ed.). (2014, des). *Luftlekkasjemåling av bygninger. hensikt og vurdering.* SINTEF Byggforsk.

Trochim, W. M. (2020, mar). *Research methods: Knowledge base.* Retrieved on 04.06.2020, from `https://conjointly.com/kb/descriptive-statistics/`

Vega Pasos, A., Zheng, X., Gillott, M., & Wood, C. (2019, 08). Experimental study on the pressure differential at which building air leakage should be measured..

Walker, I., Wilson, D., & Sherman, M. (1996). Does the power law rule for low pressure building envelope leakage? In *Proceedings of 17th aivc conference, gothenburg, sweden* (pp. 17–20).

Walker, I. S., Wilson, D. J., & Sherman, M. H. (1998). A comparison of the power law to quadratic formulations for air infiltration calculations. *Energy and Buildings*, *27*(3), 293–299.

Wikipedia contributors. (2018). *Log wind profile — Wikipedia, the free encyclopedia.* Retrieved from `https://en.wikipedia.org/w/index.php?title=Log_wind_profile&oldid=843454408` ([Online; accessed 10-March-2020])

Younes, C., Shdid, C. A., & Bitsuamlak, G. (2012). Air infiltration through building envelopes: A review. *Journal of Building physics*, *35*(3), 267–302.

Yu, J.-y., Song, K.-d., & Cho, D.-w. (2017). Resolving stack effect problems in a high-rise office building by mechanical pressurization. *Sustainability*, *9*(10), 1731.

Zheng, X., Cooper, E., Mazzon, J., Wallis, I., & Wood, C. (2019, 07). Experimental insights into the airtightness measurement of a house-sized chamber in a sheltered environment using blower door and pulse methods. *Building and Environment*, *162*, 106269. doi: 10.1016/j.buildenv.2019.106269

Zou, Y. (2010). Classification of buildings with regard to airtightness.